Dear Jason Surratt,

We have carefully considered all comments and answered all of them. We have implemented most of the suggestions and expanded the manuscript by adding box model simulations and a comparison between the a-pinene and the pinonaldehyde systems, as suggested by one of the reviewers. We also have corrected our results using a normalized pinonaldehyde turnover.

Please find the one-to-one responses to the referees with the implemented changes below.

Best regards,
Sören Zorn

All responses will be presented in Times New Roman font. The responses will appear in black, while revisions made to the manuscript will be highlighted in blue.

Reviewer 1

This manuscript examines the role of the OH-initiated H-abstraction pathway in HOM formation from α-pinene photooxidation across a systematic NO range using the SAPHIR-STAR chamber with complementary nitrate-CIMS and propylamine-CIMS. Fuzzy c-means (FCM) clustering is applied to discriminate product families by their temporal formation behavior, and parallel pinonaldehyde photooxidation experiments under matched OH/NO conditions are used to test whether secondary pinonaldehyde oxidation can account for the observed C10H15Ox-related HOM. The study makes a valuable contribution to an unresolved question in monoterpene oxidation chemistry: whether H-abstraction is a negligible curiosity or a substantive contributor to HOM and SOA under NO-rich conditions. The work extends Shen et al. (2022, Sci. Adv.) in three important ways: (i) by systematically varying NO rather than fixing it, (ii) by including a propylamine-CIMS to capture less-oxygenated products (O < 7), and (iii) by providing a direct pinonaldehyde control experiment. The experimental design is sound, the radical budget is well-constrained through a dedicated HO2 calibration via isoprene/MCM modelling, and the conclusions are generally defensible. However, a few comments should be addressed before publication.

Response:

We thank reviewer for his thoughtful review and the positive comments and have addressed all comments in detail below.

Major Comments

1. *Vereecken et al. (2007) suggested that the cleanest diagnostic of H-abstraction is the detection of C10H15Ox species with fewer than five oxygen atoms, since these cannot plausibly arise from OH-addition autoxidation chains. The authors' amine-CIMS data show exactly this: C10H15NO4 is a major peak in ANhigh but is absent from PNhigh (pinal + OH + high NO). Mechanistically, this implies a C10H15O3 peroxy radical precursor, which is the H-abstraction product from α-pinene, and it cannot arise from pinonaldehyde because pinonaldehyde H-abstraction produces C10H15O4 as the nascent RO2. This is the single most compelling piece of evidence in the manuscript and deserves to be highlighted in the abstract, elevated in Section 3.1, and emphasized in the conclusions. At present it is introduced late in Section 3.2 and treated as one observation among many.*

Responses:

We thank the reviewer for this suggestion, which will highlight our convincing evidence for the H-abstraction channel. We have revised the abstract accordingly:

1. *Revised abstract*

Highly oxygenated organic molecules (HOM) are efficiently formed via autooxidation during ·OH-initiated oxidation of α-pinene. We investigated the relative contributions of ·OH-addition and hydrogen (H)-abstraction to HOM formation from α-pinene photooxidation under varying NO conditions. HOM molecules were detected by a nitrate chemical ionization mass spectrometer (CIMS). In the absence of NO, $C_{10}H_{17}O_x$· peroxy radicals and related termination products (e.g. $C_{10}H_{18}O_x$) dominated the HOM spectrum, accounting for more than 70% of total HOM. The presence of NO substantially altered HOM products, particularly by the rapid formation of $C_{10}H_{15}O_x$·-related HOM like $C_{10}H_{15}NO_8$. The ratio of $C_{10}H_{15}NO_x$ to $C_{10}H_{17}NO_x$ increased significantly from 0.34 to 0.84 as the RO_2· loss rate via reaction with NO increased from 0.18 s^{-1} to 1.06 s^{-1}. Under high-NO conditions, $C_{10}H_{15}O_x$·-related HOM contributed up to 34% to total HOM from α-pinene oxidation systems. H-abstraction channel was proven to be the source of $C_{10}H_{15}O_x$·-related HOM. Fuzzy c-means clustering indicated that $C_{10}H_{15}O_x$·-related HOM exhibited the fastest formation rate among the identified HOM groups, consistent with first-generation products. Comparison with pinonaldehyde oxidation, obtained by normalizing HOM yields to pinonaldehyde turnover, suggests that pinonaldehyde contributed ~5% of HOM in α-pinene systems, excluding secondary oxidation as the dominant source. Detection of $C_{10}H_{15}NO_4$ under high-NO conditions by propylamine-CIMS is indicator for formation of $C_{10}H_{15}O_3$· peroxy radicals, formed by alkoxy radical decomposition and six-membered ring opening in H-abstraction channel. This study highlights the role of the H-abstraction pathway in OH-initiated α-pinene oxidation under NO-influenced conditions and provides new constraints on detailed HOM formation mechanisms.

We have also revised the conclusions accordingly:

2. *Revised Conclusions:*

In this study a series of photooxidation experiments was conducted under varying NO levels to investigate the effect of NO on the $C_{10}H_{15}O_x$·-related HOM formation in the α-pinene photooxidation system, and to unravel potential formation pathways of these products. The chemical system was brought to a steady state in the dark. Afterwards, reactions were initiated by photolyzing H_2O_2. We focused on early reaction stages (the first hundreds of seconds), during which RO_2· + NO reactions and RO_2· autoxidation reactions dominate the fate of the RO_2·. $C_{10}H_{17}O_x$·-related HOM are dominantly formed via the ·OH·-addition pathway. Product distributions, potential formation pathways, and rates of $C_{10}H_{17}O_x$·-related HOM have been widely and extensively studied (Berndt, 2021; Xu et al., 2019), and our findings on $C_{10}H_{17}O_x$·-related HOM formation are consistent with previous studies. However, potential formation pathways, distributions, and NO dependence of $C_{10}H_{15}O_x$·-related compounds derived from H-abstraction channel were missing systematic exploration so far.

To constrain the potential contribution of H-abstraction to HOM formation, regimes with and without NO were directly compared, and a separate experiment of pinonaldehyde oxidation under similar conditions was performed. Additionally, measurements by Amine-CIMS were used to detect less oxygenated products. Since the photolysis of H_2O_2 was utilized to produce ·OH radicals O_3 did not accumulate during the early reaction stages; therefore, ozonolysis did not interfere with the ·OH pathways. FCM analysis proves that the dominant species in the $C_{10}H_{15}NO_x$ family, $C_{10}H_{15}NO_8$ and $C_7H_9NO_8$, can be distinguished from other species by their fast formation rates in the presence of NO. Pinonaldehyde oxidation can only contribute ~ 5% to HOM formation in α-pinene oxidation systems. Therefore, neither ozonolysis nor secondary oxidation can explain the significant formation of $C_{10}H_{15}O_x$·-related HOM, which points to H-abstraction from α-pinene by ·OH being the most likely formation pathway.

As illustrated in ***Figure S12*** and ***Figure S15,*** the contribution of the H-abstraction pathway to HOM formation increases with elevated NO levels compared to the ·OH addition pathway. The ratios between major $C_{10}H_{15}O_x$·-related HOM and $C_{10}H_{17}Ox$·-related HOM rise with increasing NO concentrations. The ratios of $C_{10}H_{15}O_x$· peroxy radicals to $C_{10}H_{17}O_x$· peroxy radicals are 0.06, 0.83, and 1.42 under NO-free, low-NO, and high-NO conditions, respectively. Similarly, the ratio of $C_{10}H_{15}NO_x$ to $C_{10}H_{17}NO_x$ increases from 0.34 to 0.84 when NO levels increase from low to high. The sum of major $C_{10}H_{15}O_x$·-related closed-shell HOM products ($C_{10}H_{14}O_x$, $C_{10}H_{15}NO_x$ and $C_{10}H_{16}O_x$) contributes 24% and 34% under low-NO and high-NO conditions, while being negligible under NO-free conditions.

The contribution of H-abstraction related products observed in this study was lower than that reported by Shen and coworkers, who reported a contribution of more than 70% (Shen et al., 2022). The experiments from the two studies were conducted in different chambers, under different conditions and with different instrumentations applied. Two chambers could introduce different wall losses of HOM, which can be further different between less oxygenated HOM and highly oxygenated HOM.

In this study the ·OH radicals were generated via photolysis of H_2O_2, whereas HONO photolysis was the main source of ·OH in Shen et al. (2022). The consecutive reaction between ·OH and H_2O_2 in our experiments leads to an enhanced production of HO_2· radicals, resulting in an HO_2· concentration of ~4×10^8 molecule cm^{-3}, which is approximately one order of magnitude higher than that reported by Shen et al. (2022). Also, the NO concentration in Shen et al. was constantly around ~20 ppb, while it was only ~7 ppb before reaction in our study, resulting in a concentration of ~1 ppb during the early-reaction stage. Despite these differences, the contributions of RO_2· + NO reactions are dominant in both studies, accounting for more than 95% of RO_2· biomolecular losses under high-NO conditions. In addition, we did only consider early reaction stages, during which secondary oxidation was negligible and RO_2· chemistry was dominated by autoxidation and RO_2· + NO reactions. Therefore, the chemical system can be expected to be similar for both studies, at least under high-NO conditions. However, the constantly higher level of NO in the study by Shen et al. (2022) may continuously promote the H-abstraction channel.

The discrepancy may also arise from differences in measurement techniques: Shen et al. (2022) used an Eisele type inlet (Mauldin et al., 1999), while in this study a MION inlet was used (Rissanen et al., 2019). To compare both inlet systems, we conducted an experiment where both types of inlets were simultaneously used to measure the same oxidation systems. The reference system was α-pinene oxidation by ·OH, with the addition of NO (***Figure S17).*** The results indicate that the MION inlets detects a larger fraction of lesser oxygenated HOM (less than eight oxygen atoms) than the Eisele inlet, and that these HOM dominate the $C_{10}H_{17}O_x$·-related HOM family, while the relative contribution of higher oxygenated HOM (more than eight oxygen atoms) was larger in the study by Shen et al. (2022). When only the highly oxygenated HOM compounds are considered as was done in the study be Shen and coworkers, the relative contribution of $C_{10}H_{15}O_x$·-related HOM to the total HOM does increase to 64%. Therefore, a deeper comparison of the two inlet types may be of interest in the future but is outside the scope of this study.

These findings indicate that the HOM yield attributed to the H-abstraction pathway compared to the ·OH addition pathway can be significant, and should not be overlooked when assessing the importance of HOM in SOA formation, especially in the presence of NO. Comprehensive product distributions formed through the H-abstraction pathway in α-pinene oxidation are illustrated in this study. HOM species with the formula $C_{10}H_{15}NO_8$, recognized as characteristic indicators of ·OH-initiated monoterpene oxidation in presence of NO under daytime atmospheric conditions (Yan et al., 2016; Kulmala et al., 2013), may potentially be attributed to the H-abstraction pathway. However, even the NO concentrations in the low-NO case of this study were higher than those typically observed at Hyytiälä. Therefore, the significance of the H-abstraction pathway under typical low-NO boreal forest conditions remains uncertain and requires further investigation. In contrast, the contribution of the H-abstraction channel to HOM formation is expected to be more pronounced in megacities supposed to be under high NO conditions. The presence of NO not only terminates peroxy radicals and suppresses HOM formation, but also propagates the oxidative radical chain through the formation of alkoxy radicals and their subsequent isomerization, a process that under high NO levels can even compete with autoxidation (Kang et al., 2025). These reactions lead to effective NO-NO_2 conversion and can then become a crucial step to promote O_3 formation. The occurrence of alkoxy steps can also directly be related to O_3 formation in addition to O_3 sensitivity via the ratio of organic nitrate and non-nitrate HOM (Zhang et al., 2024). However, branching ratios towards alkoxy radical formation remain uncertain, when RO_2· reacts with NO. Further investigation is needed to clarify the role of alkoxy processes in both SOA and O_3 formation.

2. *The authors exclude ozonolysis and pinonaldehyde oxidation (via the FCM timing and the PNhigh control). However, a mechanistic alternative receives little attention: alkoxy radicals derived from C10H17Ox + NO can undergo H-shifts, β-scissions, or HO2 loss steps that might produce 15-H*

skeletons. This is particularly relevant for the ~75% of four-membered-ring-retained C10H17O3 isomers whose fate under high NO is not extensively discussed here. The authors should (i) explicitly consider whether alkoxy-mediated conversion of C10H17Ox into C10H15Ox products can be quantitatively excluded and (ii) provide an estimate of the contribution this pathway could make given the measured alkoxy branching. The text on lines 262–268 acknowledges alkoxy propagation in the C10H17Ox family but does not connect it to the possibility of subsequent C10H15Ox formation.

Responses:

We thank the reviewer for this comment. However, we can exclude formation of C10H15Ox related alkoxy radicals from the reaction of C10H17Ox with NO for the early experimental stages.

Neither H-migration nor beta-scission in the alkoxy radials will lead to H-loss without breaking the C-C bond, and the resulting alkyl radical will add O2, thus re-starting the C10H17Ox autoxidation chain. $HO_2\cdot$ loss is also unlikely to happen for these molecules as both, H-migration and scission are expected to be favorable (Vereecken and Peeters, 2009, 2010), it takes place it will lead to the formation of a carbonyl and $HO_2\cdot$, resulting in the loss of one H-atom and subsequent formation of C10H16Ox products. While these could in principle react via H-abstraction, leading to C10H15Ox intermediates, this will occur on timescales relevant only for secondary chemistry. For analog reasons it also cannot be an important source for pinonaldehyde. Regarding the contribution of the oxidation of pinonaldehyde to C10H15Ox-derived HOM products, please read our answer to ***Comment 3,*** where we explain in detail why pinonaldehyde oxidation can only contribute up to 10% to the HOM formation in α-pinene oxidation systems.

To clarify this, we extended the related discussion in the manuscript in lines 383-398:

Alkoxy radicals derived from reactions involving $C_{10}H_{17}O_x\cdot$ peroxy radicals and NO can undergo an H-shift, β-scissions, or $HO_2\cdot$ loss steps; however, none of these reactions are expected to form $C_{10}H_{15}O_x\cdot$ peroxy radicals directly. For example, neither H-migration nor β-scission will lead to the loss of a hydrogen atom without a carbon-carbon bond cleavage, and the resulting alkyl radicals will react efficiently with O_2 to regenerate $C_{10}H_{17}O_x\cdot$ radicals and thus continue the autooxidation cycle. The $HO_2\cdot$ loss channel is expected to be a minor pathway for the considered alkoxy radicals, because intramolecular H-migration and β-scission are more favorable, as previously shown by Vereecken and Peeters (Vereecken and Peeters, 2009, 2010). If $HO_2\cdot$ loss channel would happen, it would lead to the formation of carbonyl and $HO_2\cdot$, losing one hydrogen atom forming $C_{10}H_{16}O_x$ products. While the $C_{10}H_{16}O_x$ products could, in principle, react with ·OH radical again to produce $C_{10}H_{15}O_x\cdot$ intermediates, this process would occur on the timescale of secondary chemistry and is therefore unlikely to contribute significantly during the early reaction stages. Pinonaldehyde was dominant among $C_{10}H_{16}O_x$ compounds, but its oxidation cannot become a significant source of $C_{10}H_{15}O_x\cdot$-related HOM, which will be discussed in Section 3.2.

3. *The current argument in Section 3.2 compares summed signals and distributions qualitatively between ANhigh and PNhigh. The authors are suggested to scale the PNhigh yields (per unit pinonaldehyde turnover) by the actual pinonaldehyde concentration and turnover in the ANhigh experiment. Whatever remains must be attributed to primary H-abstraction (or to another non-pinonaldehyde pathway). This arithmetic would transform a qualitative argument into a quantitative upper-bound statement and should be included. Relatedly, the amine-CIMS ratio for C10H15NOx between ANhigh and PNhigh (0.56×) is currently glossed over; because it is less than unity, it seemingly argues for a meaningful pinonaldehyde contribution to the less-oxygenated component, and this deserves an explicit inclusion.*

Responses:

We thank the reviewer for this comment. We agree that normalizing major product intensities by the pinonaldehyde turnover of each experiment provides a more appropriate basis for evaluating the contribution of pinonaldehyde oxidation to the formation of C10H15Ox-related HOM observed during α-pinene oxidation.

Previously, we did not calculate the absolute turnover for all the experiments. For the α-pinene oxidation under high-NO conditions and the pinonaldehyde oxidation under high-NO conditions, the turnover ratio was estimated and described as, *'The estimated pinonaldehyde turnover under PN_{high} conditions is ~11 times the turnover as product under AN_{high} conditions.'* Therefore, although the ratio for C10H15NOx between α-pinene case and pinonaldehyde case was ~ 0.56, the pinonaldehyde turnover in pinonaldehyde experiment is much higher than it in α-pinene experiment. Overall, the pinonaldehyde contribution was negligible.

To highlight this evidence and make the comparison between the α-pinene case and the pinonaldehyde case clearer and more convincing, we have made several revisions:

1. We performed model simulations for both the α-pinene-high NO and the pinonaldehyde-high NO experiments to estimate ·OH radical concentrations during the early stages. These simulations were subsequently used to estimate the pinonaldehyde turnover in each experiment, which was shown in Figure 5a (which was previously Figure 4a).
2. We subsequently revised Figure 5b by normalizing the major product intensity by the ratio of the pinonaldehyde turnover obtained from the α-pinene case and the pinonaldehyde case. The updated Figure 5b now shows the average intensities of major products from these two experiments, with the corrected pinonaldehyde turnover.
3. Furthermore, we have expanded the discussion in the manuscript to clarify the normalization procedure and to explicitly account for differences in ·OH exposure and precursor reactivity when evaluating the role of pinonaldehyde oxidation in the formation of C10H15Ox-related HOM. In

summary, we found that the oxidation of pinonaldehyde during the α-pinene oxidation experiments did contribute less than 10% to C10H15Ox-related HOM.

We have updated the figures and text in the manuscript as shown below:

To assess the potential contribution of pinonaldehyde oxidation to the formation of $C_{10}H_{15}O_x$·-related HOM, pinonaldehyde photooxidation experiments were conducted under NO-free and high-NO conditions, analogous to conditions applied in the α-pinene systems (***Table 1***). Time series of α-pinene and its oxidation product pinonaldehyde during the first 30 min of the α-pinene (high-NO) experiment are shown in Figure ***5(a-1).*** The corresponding turnovers of α-pinene and pinonaldehyde are presented in Figure ***5(a-1).*** Similarly, the concentration of pinonaldehyde and its turnover during the pinonaldehyde (high-NO) experiment are shown in Figure ***5(a-2).*** ·OH concentrations were estimated using model simulations.

During early stage, the average pinonaldehyde turnover was 8.9×10^6 molecules cm^{-3} s^{-1} under pinonaldehyde (high-NO) condition, approximately 6 times higher than the turnover (1.5×10^6 molecules cm^{-3} s^{-1}) under α-pinene (high-NO) condition. To facilitate comparison between the two experiments, we calculated the pinonaldehyde turnover for both experiments and compared it to obtain the ratio between the high-NO α-pinene and pinonaldehyde experiment (hereafter referred to as the pinonaldehyde turnover ratio). Signals measured in the pinonaldehyde experiment were subsequently normalized by this ratio to account for differences in the pinonaldehyde turnover between the two experimental systems. The distributions of major $C_{10}H_{15}O_x$·-related products observed during the high-NO α-pinene and high-NO pinonaldehyde experiments are presented in Figure 5(b). Major products belonging to the $C_{10}H_{14}O_x$ and $C_{10}H_{15}NO_x$ family detected by both nitrate-CIMS (N) and amine-CIMS (A) are included. The data shown in ***Figure 5(b)*** represents averages over the first 320 s following the initiation of oxidation, corresponding to the early reaction stage, during which RO_2· + NO accounts for more than 90% of the total bimolecular RO_2· loss rate. In addition, all product signals here as well as all data used for comparison in the following paragraphs have been normalized by the pinonaldehyde turnover.

The pinonaldehyde turnover ratio during the first 320 s exceeded 5 and was substantially higher during the first 100 s. This large difference arises because pinonaldehyde was present at the start of the pinonaldehyde high-NO experiment and was therefore immediately available for reaction with ·OH. In contrast, under α-pinene high-NO conditions, pinonaldehyde had to be formed through α-pinene oxidation before it could undergo further reactions, resulting in a much lower pinonaldehyde turnover during the early stages of the experiment. For $C_{10}H_{15}O_x$·-related HOM detected by nitrate-CIMS the summed signals of the $C_{10}H_{14}O_x$ and $C_{10}H_{15}NO_x$ families under α-pinene high-NO conditions exceed those of pinonaldehyde high-NO conditions by factors of approximately 20 and 10, respectively. Although pinonaldehyde oxidation contributes to the formation of $C_{10}H_{15}O_x$·-related HOM under high-NO conditions, this contribution is minor and can explain approximately 5% of the HOM yield observed from

α-pinene oxidation. Similarly, for less oxygenated products measured by amine-CIMS, the summed concentrations of the $C_{10}H_{14}O_x$ and $C_{10}H_{15}NO_x$ families were 98 times higher in the α-pinene high-NO experiment, and 6.7 times higher in the pinonaldehyde high-NO experiment.

For highly oxygenated compounds detected by nitrate-CIMS, species containing more than 10 oxygen atoms account for 11% of the $C_{10}H_{14}O_x$ family and for 13% of the $C_{10}H_{15}NO_x$ family under α-pinene high-NO condition, whereas their contributions are much lower for pinonaldehyde high-NO conditions (3% and 5%, respectively).

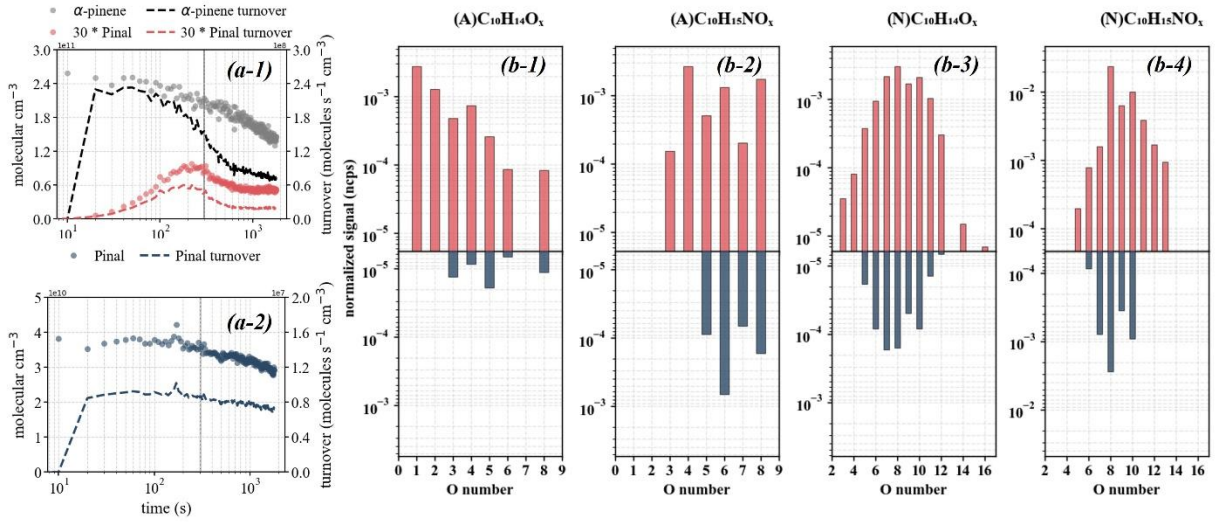

Figure 5. Panel (a-1) displays concentrations and turnover of α-pinene and pinonaldehyde (Pinal) during α-pinene photooxidation under high-NO conditions, while panel (a-2) represents concentrations and turnover of pinonaldehyde during the high-NO pinonaldehyde photooxidation experiment. Major product distributions are shown in panel (b-1) to (b-4). Signals detected in the pinonaldehyde experiment are normalized by the ratio of the pinonaldehyde turnover during the pinonaldehyde experiment to the respective turnover during the α-pinene experiment. The products are separated into four groups: (A)$C_{10}H_{14}O_x$, (A)$C_{10}H_{15}NO_x$, (N)$C_{10}H_{14}O_x$, (N)$C_{10}H_{15}NO_x$, of which (A) and (N) represent signals derived from amine-CIMS and nitrate-CIMS, respectively. Data from α-pinene oxidation and pinonaldehyde oxidation are colored in pink and blue, respectively.

4. *The inference of generation order from cluster peak times (160, 210, 290, 850 s for clusters 1–4) is central to the argument that C10H15NO7/NO8 are first-generation products and that pinonaldehyde (in cluster 3) cannot be their precursor. Several uncertainties are not addressed: (1) The four-cluster solution was selected from SSE, distortion, and silhouette curves (Figure S5), but robustness of the cluster-1 membership of C10H15NO7/NO9 under 3- and 5-cluster solutions should be tested. (2) Early-peaking behavior does not strictly imply first-generation status; species formed rapidly from short-lived precursors can also peak early. (3) The FCM run of 50 initializations per cluster number*

presumably yields a distribution of cluster assignments; the authors should report how stable cluster-1 membership is across these initializations.

Responses:

We thank the reviewer for the comments and suggestions. We have extensively tested the clustering with several possible cluster solutions and varying parameters to check the stability of clustering results, analog to the procedure previously developed and described in (Wu et al., 2024). We will discuss the previously obtained results from the 3- and 5-cluster solutions here and have also included them in the manuscript and the supplemental material, as suggested by the reviewer.

When investigating 3- and 5-cluster solutions we found that the conclusions from the manuscript remain, meaning that the HOM indicators derived from the H-abstraction channel (e.g., C10H15NO8 and C7H9NO8) were always attributed to the first emerging cluster. The results of 3-cluster solution and 5-cluster solution are shown below.

Regarding (2): in our manuscript (analog to definitions often used in atmospheric chemistry), first-generation products are defined as closed-shell species formed directly from the initial oxidation of the precursor, without subsequent oxidation steps. In this framework, the temporal evolution of a compound is determined by both its formation and loss processes. For HOM we consider wall-loss as the dominant sink for our experimental conditions. While wall-loss rates may vary to some extent among compounds, such differences are expected to be smaller than the variability in formation rates under the same conditions. Therefore, the observed differences in time profiles are primarily interpreted as reflecting differences in formation rates. Under this assumption, compounds exhibiting earlier signal maxima are associated with faster formation and thus more likely represent first-generation products.

To test the stability of the clustering results, as suggested in (3), we ran the clustering 50 times with different initializations for the four-cluster solution, and investigated the cluster assignment for all key compounds, such as $C_{10}H_{15}NO_8(NO_3^-)$, $C_7H_9NO_8(NO_3^-)$ and $C_{10}H_{16}O_2(C_3H_7NH_3^+)$. The results demonstrated a very high clustering stability, as these compounds were consistently assigned to the same cluster across all runs. For example, $C_{10}H_{15}NO_8(NO_3^-)$ was assigned to the first cluster in all clustering runs. Therefore, the clustering results and insights derived from them are highly robust and reliable.

Below we attached the text and figures which were added to the manuscript and the supplement. Revised or added text is shown in blue.

To assess the robustness of the clustering results, additional cluster analysis was performed using a three- and five-cluster solution, as shown in ***Figure S6*** and ***Figure S7***, respectively. Consistent conclusions are obtained regardless of the number of clusters specified. In particular, the key compounds derived from the H-abstraction channel, such as $C_{10}H_{15}NO_8(NO_3^-)$ and $C_7H_9NO_8(NO_3^-)$, were consistently assigned to the first cluster with the fastest formation rate. The stability of the clustering results was

further evaluated by performing 50 clustering runs with random initializations and using the four-cluster solution. The distributions of the cluster assignments were then analyzed, as shown in ***Figure S8***, with particular attention given to the key compounds discussed above, including $C_{10}H_{15}NO_8(NO_3^-)$, $C_7H_9NO_8(NO_3^-)$, and $C_{10}H_{16}O_2(C_3H_7NH_3^+)$. The results demonstrate the high stability of the cluster solution, as these compounds were consistently assigned to the same cluster across all runs. For example, $C_{10}H_{15}NO_8(NO_3^-)$ was assigned to the first cluster in all runs. Therefore, the clustering results and insights derived from them are highly robust and reliable.

The compounds $C_{10}H_{15}NO_7(NO_3^-)$ and $C_{10}H_{15}NO_8(NO_3^-)$ are assigned to cluster 1 with the fastest formation rate; thus, they are likely first-generation products.

Changes added to the supplemental information:

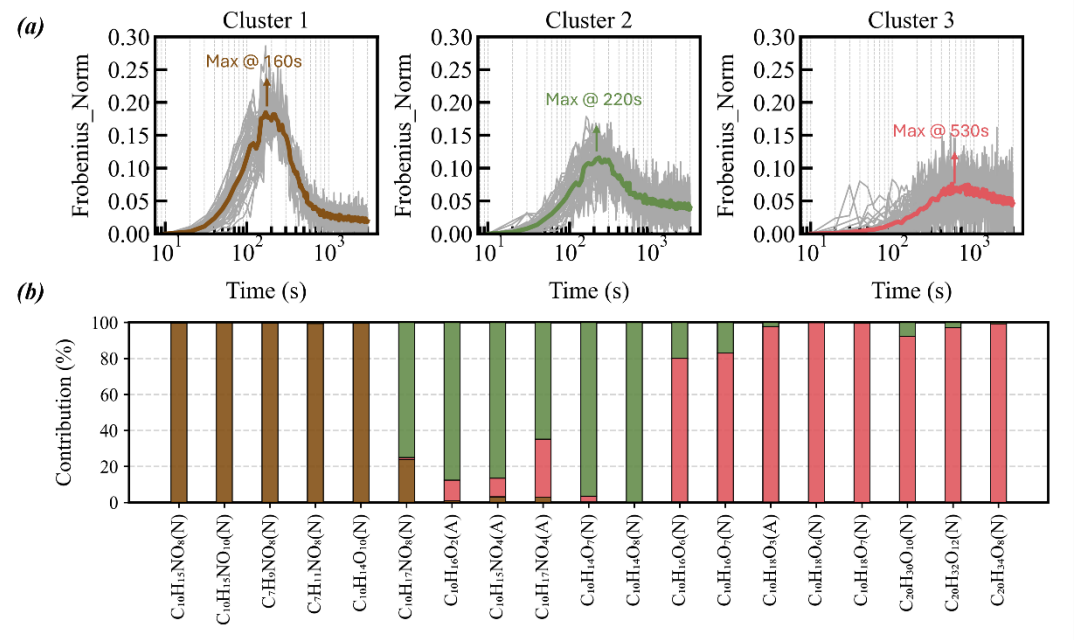

Figure S13. Results of fuzzy c-means clustering for three clusters for the dominant signals (156 in total) during early reaction stages of α-pinene photooxidation under high-NO condition are shown in panel ***(a)***. The time series of the cluster centers are displayed as colored solid lines, while individual contributing species are shown as gray lines. Panel ***(b)*** illustrates the cluster apportionment of selected major products detected in both nitrate-CIMS (N) and amine-CIMS (A).

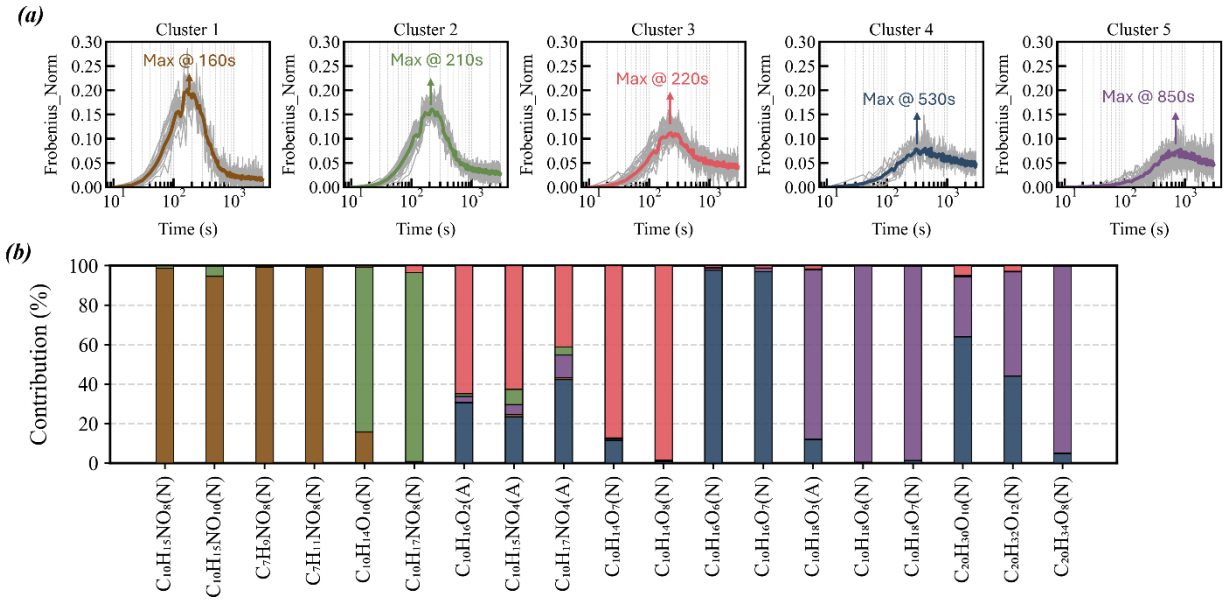

Figure S14. Results of fuzzy c-means clustering for five clusters for the dominant signals (156 in total) during early reaction stages of α-pinene photooxidation under high-NO condition are shown in panel ***(a)***. The time series of the cluster centers are displayed as colored solid lines, while individual species are shown as gray lines. Panel ***(b)*** illustrates the cluster apportionment of selected major products detected in both nitrate-CIMS (N) and amine-CIMS (A).

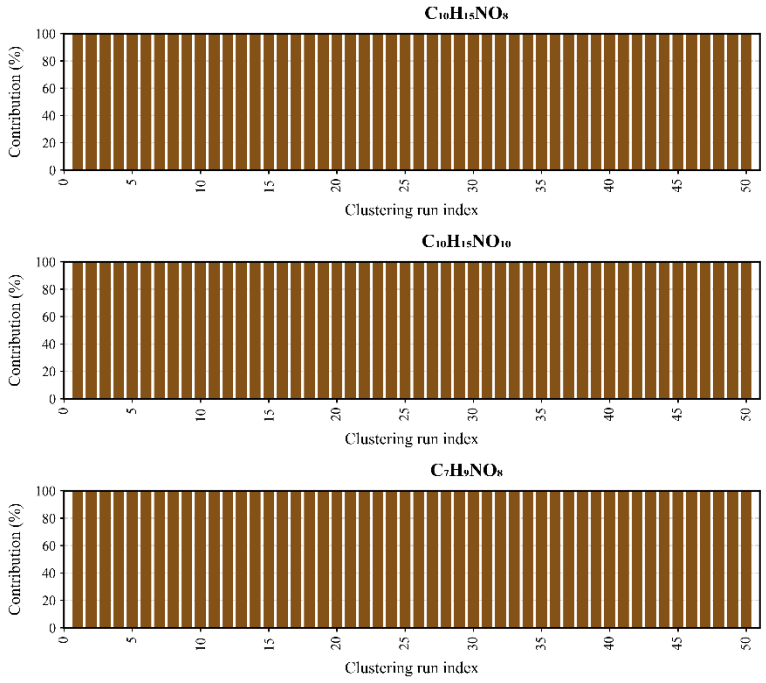

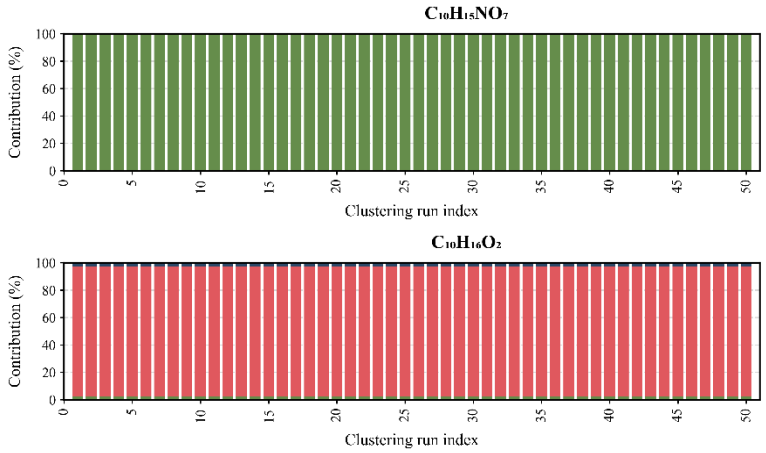

Figure S15. The results of 50 independent clustering runs using a four-cluster solution and random initialization are shown. The distributions of cluster assignments for key compounds are evaluated, including $C_{10}H_{15}NO_8(NO_3^-)$, $C_{10}H_{15}NO_{10}(NO_3^-)$, $C_7H_9NO_8(NO_3^-)$, $C_{10}H_{15}NO_7(NO_3^-)$, and $C_{10}H_{16}O_2(C_3H_7NH_3^+)$.

5. *The H-abstraction contribution reported here (~30% of HOM under ANhigh) is described as "70% lower than" Shen et al. The proposed explanation (Eisele inlet vs. MION inlet detection efficiency for less-oxygenated C10H17Ox-related HOM) is highly speculative. The two studies also differ in chamber, residence time, NO range, VOC concentration, and OH source. A more detailed discussion would be helpful.*

Responses:

We thank the reviewer for this insightful comment. We agree that the comparison with Shen et al. should be interpreted with more caution, as the two studies were conducted under different experimental conditions. In the revised manuscript, we have expanded the discussion and now explicitly address several factors that may contribute to the discrepancy, including differences in reaction time, RO2 fates under high-NO conditions, and instrumental setup.

Although we performed experiments with different ·OH sources, the level of and exposure to ·OH are comparable between the two experiments. In the experiments presented in the manuscript, more $HO_2\cdot$ radicals were produced due to the reaction between H_2O_2 and OH, resulting in $HO_2\cdot$ concentrations which were around one order of magnitude higher than those in Shen et al.'s study. However, box model simulations we performed show that under high-NO conditions the $RO_2\cdot$ + NO reaction rate can explain more than 95% of bimolecular $RO_2\cdot$ losses, which is consistent with Shen et al. Since only early-reaction stages were considered for both studies, during which secondary oxidation is negligible, and $RO_2\cdot$ + NO dominate $RO_2\cdot$ biomolecular reactions, the chemical regimes of both studies are very similar and

comparable. The different chamber setups have different wall loss rates, which can lead to larger uncertainties for determining and comparing HOM yields and product distributions.

Regarding the proposed explanation related to the inlet systems, we agree that the interpretation was insufficiently described and supported in the previous version of our manuscript. To strengthen this discussion, we now include evidence from previous intercomparisons and measurements that were specifically designed to evaluate the performance of an Eisele and a MION inlet system. The measurements suggest that the detection efficiency for less-oxygenated HOM (O<8) differs between the two inlet configurations. For example, less-oxygenated C10H17Ox-related HOM were detected with higher efficiency by the MION inlet (***Figure S17***). Therefore, the relative contribution of C10H15Ox-related HOM might be higher in the Eisele inlet. Since this study used a MION inlet, whereas Shen et al. used an Eisele inlet, inlet-dependent sensitivity differences could partly explain the lower contribution of H-abstraction-related products observed in this study.

We extended the discussion and added one more plot to show the different measurement results between the Eisele and the MION inlet (Figure S17):

The contribution of H-abstraction related products observed in this study was lower than that reported by Shen and coworkers, who reported a contribution of more than 70% (Shen et al., 2022). The experiments from the two studies were conducted in different chambers, under different conditions and with different instrumentations applied. Two chambers could introduce different wall losses of HOM, which can be further different between less oxygenated HOM and highly oxygenated HOM.

In this study the ·OH radicals were generated via photolysis of H_2O_2, whereas HONO photolysis was the main source of ·OH in Shen et al. (2022). The consecutive reaction between ·OH and H_2O_2 in our experiments leads to an enhanced production of HO_2· radicals, resulting in an HO_2· concentration of ~4 × 10^8 molecule cm^{-3}, which is approximately one order of magnitude higher than that reported by Shen et al. (2022). Also, the NO concentration in Shen et al. was constantly around ~20 ppb, while it was only ~7 ppb before reaction in our study, resulting in a concentration of ~1 ppb during the early-reaction stage. Despite these differences, the contributions of RO_2· + NO reactions are dominant in both studies, accounting for more than 95% of RO_2· biomolecular losses under high-NO conditions. In addition, we did only consider early reaction stages, during which secondary oxidation was negligible and RO_2· chemistry was dominated by autoxidation and RO_2· + NO reactions. Therefore, the chemical system can be expected to be similar for both studies, at least under high-NO conditions. However, the constantly higher level of NO in the study by Shen et al. (2022) may continuously promote the H-abstraction channel.

The discrepancy may also arise from differences in measurement techniques: Shen et al. (2022) used an Eisele type inlet (Mauldin et al., 1999), while in this study a MION inlet was used (Rissanen et al., 2019). To compare both inlet systems, we conducted an experiment where both types of inlets were simultaneously used to measure the same oxidation systems. The reference system was α-pinene oxidation

by ·OH, with the addition of NO (***Figure S17).*** The results indicate that the MION inlets detects a larger fraction of lesser oxygenated HOM (less than eight oxygen atoms) than the Eisele inlet, and that these HOM dominate the $C_{10}H_{17}O_x$·-related HOM family, while the relative contribution of higher oxygenated HOM (more than eight oxygen atoms) was larger in the study by Shen et al. (2022). When only the highly oxygenated HOM compounds are considered as was done in the study be Shen and coworkers, the relative contribution of $C_{10}H_{15}O_x$·-related HOM to the total HOM does increase to 64%. Therefore, a deeper comparison of the two inlet types may be of interest in the future but is outside the scope of this study.

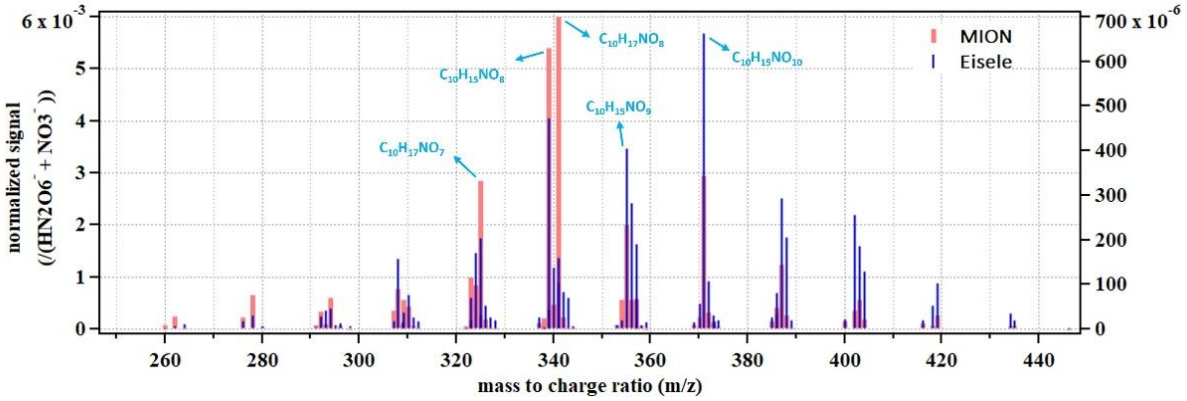

Figure S17. The signal of products derived from α-pinene oxidation with NO injection, detected by CIMS coupled with the MION (pink) and Eisele (blue) inlets.

6. *HO2 varies by a factor of ~3 across conditions. Because HO_2· is a competing sink for both C10H17Ox and C10H15Ox and because the C10H16Ox family assignment explicitly invokes C10H15Ox + HO2, the varying HO2 should be more prominently incorporated into the interpretation of C10H15Ox-related HOM yields. It would be useful to present yields normalized by the relevant rate-weighted sink flux rather than by raw VOC turnover.*

Responses:

We thank the reviewer for this comment. We agree that RO_2· + HO_2· reactions are an important termination pathway for RO_2· radicals and can influence the product distribution and thereby potentially the yields of C10H15Ox-related HOM. For the C10 monomer HOM investigated here, both C10H14Ox and C10H15NOx are expected to originate from C10H15Ox radicals. We have shown above that the H-abstraction pathway is the dominant source of these C10H15Ox radicals.

In addition, some compounds within the C10H16Ox group may also be formed through termination reactions of C10H15Ox radicals, for example via C10H15Ox + HO_2· → C10H16Ox or C10H15Ox + RO_2· → C10H16Ox (-OH). Compounds assigned to the C10H16Ox group can also be produced from

C10H17Ox radicals through termination reactions such as C10H17Ox + RO_2· → C10H16Ox (=O). Therefore, it is difficult to unambiguously distinguish whether a given C10H16Ox compound originates from C10H15Ox or C10H17Ox radicals solely based on our measurements. Consequently, a quantitative separation of the C10H16Ox group into products derived from these two radical pathways would come with high uncertainties.

Like the formation pathways of C10H16Ox, which involves C10H15Ox, C10H18Ox can also be produced when C10H17Ox reacts with RO_2· and HO_2· radicals. If we assume similar bimolecular reaction rate constants for C10H15Ox and for C10H17Ox with NO, HO_2·, and RO_2·, and further that the RO_2· fate is the same for these product classes under comparable conditions, then the loss pathways of C10H15Ox and C10H17Ox can be also considered similar. Under these assumptions, the ratio of C10H18Ox to C10H17NOx can be approximated as equivalent to the ratio of C10H16Ox (derived from C10H15Ox) to C10H15NOx. This relationship may provide a potential approach to estimate the partitioning of C10H16Ox compounds into two groups.

Therefore, to elucidate the contribution of H-abstraction to HOM yields under varying RO_2· fates, we performed box model simulations to estimate the radical concentrations during the early reaction stages, and then tried to quantitively estimate the relative contributions of the different biomolecular reactions of RO_2· + HO_2·, RO_2· + RO_2·, and RO_2· + NO to the total biomolecular losses for all RO_2·. Based on the results from the simulations and estimates, contributions of C10H15Ox-related HOM are negligible for conditions without NO while contributing ~24% and ~34%, for low-NO and high-NO conditions, respectively.

To emphasize and clarify these conclusions we added descriptions about the model simulations and the definitions of early reaction stages to the manuscript. Additionally, the conclusions about the contributions of C10H15Ox-related HOM were revised accordingly.

The updated figures and text to determine RO_2· fates under different conditions are attached below:

Model simulations to determine early reaction stages

To clarify the role of the H-abstraction channel under varying NO conditions the early reaction stages are particularly relevant. In this study, we define early reaction stages using three criteria: (i) α-pinene turnover exceeds that of pinonaldehyde by a factor of ten, (ii) under conditions with NO, biomolecular reactions of RO_2· are dominated by RO_2· + NO and contribute more than 90% to the biomolecular loss of RO_2·, and (iii) α-pinene oxidation is primarily driven by OH· rather than O_3. Therefore, model simulations for α-pinene photooxidation systems were conducted to quantitively identify these early reaction stages.

As shown in ***Figure 2 (a-1) to (c-1)***, the model captures the evolution of the system quite well but generally underestimates NO and O_3 concentrations. These discrepancies may arise from differences in the temporal resolution of measurements and simulations, physical effects introduced by the activation of the UVC lamps (e.g., changing emissions due to temperature adjustment of the UVC lamp), and uncertainties

in the chemical mechanism including reactions currently not represented in the model framework. The HO_2· and RO_2· concentrations obtained from the simulations are shown in ***Figure 2 (a-2) to (c-2)*** together with the relative contributions of RO_2· + NO, RO_2· + HO_2· and RO_2· + NO to the total biomolecular RO_2 loss. Here, the reaction rates were calculated with $k_{[RO2][HO2]} = 1.85 \cdot 10^{-11}$ cm^3 s^{-1}, $k_{[RO2][NO]} = 1 \cdot 10^{-11}$ cm^3 s^{-1} and $k_{[RO2][RO2]} = 5 \cdot 10^{-12}$ cm^3 s^{-1} (Baker et al., 2024; Berndt et al., 2016; Jenkin et al., 1997).

Based on these results, reactions occurring within the first 100 s, 100 s, and 320 s after initiation of reactions by starting the photooxidation were defined as early stages for the NO-free, low-NO, and high-NO conditions, respectively. The average bimolecular reaction rates for RO_2· + NO were negligible for cases without NO and increased to 0.179 s^{-1} and 1.06 s^{-1} for the low-NO and high-NO conditions, respectively. For RO_2· + HO_2· reactions, the rates were 0.0055 s^{-1}, 0.011 s^{-1}, and 0.0075 s^{-1}, while those for RO_2· + RO_2· reactions were 0.0075 s^{-1}, 0.0029 s^{-1}, and 0.0014 s^{-1} for NO-free, low-NO, and high-NO conditions, respectively. The contribution of RO_2· + NO was higher than 90% under both low-NO and high-NO conditions.

For pinonaldehyde photooxidation under high-NO conditions, the reactions within the early reaction stages were also investigated to facilitate comparison with the corresponding α-pinene system under high NO conditions. Besides H-abstraction channel, reactions of α-pinene with O_3, and pinonaldehyde with ·OH may also contribute to the formation of $C_{10}H_{15}O_x$ radicals. Therefore, the loss of α-pinene due to oxidation by O_3 formed as a byproduct of other reactions, and the loss of pinonaldehyde via OH oxidation, were evaluated. The results are shown in detail in ***Figure S5***. In both cases, losses are smaller than 10% of the reaction rate of α-pinene with OH·, which further supports our definition of early reaction stage being reasonable and representative.

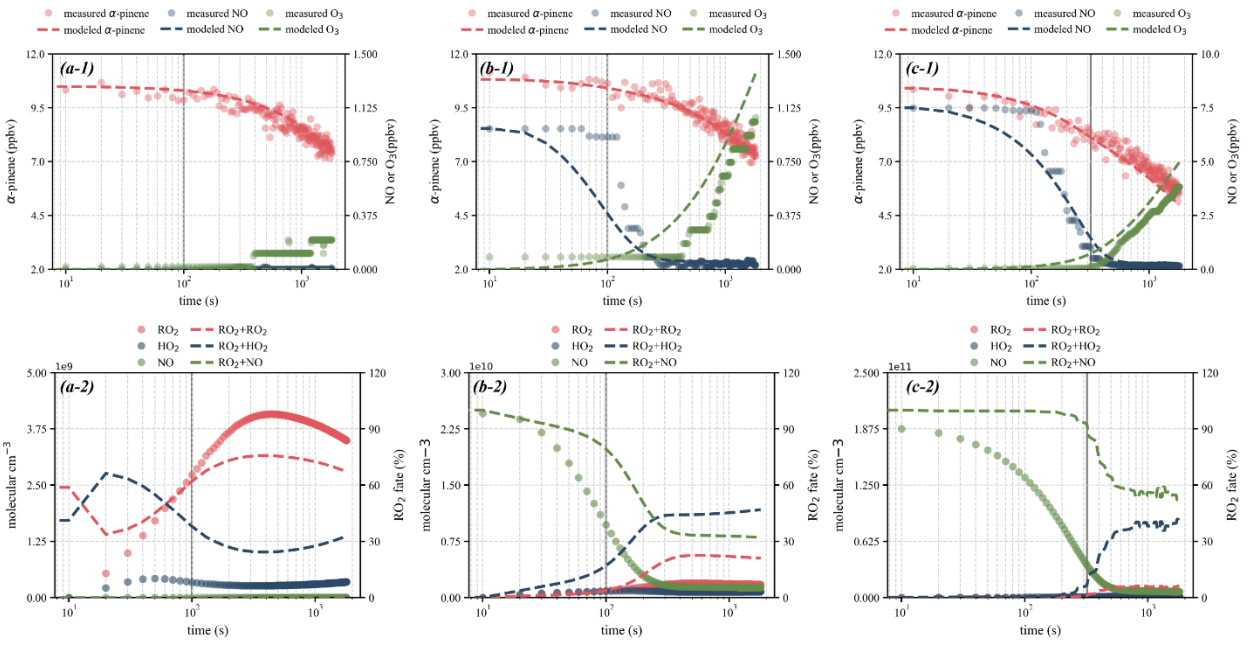

Figure 2. Results of model simulations for α-pinene photooxidation under NO-free (a-1, a-2), low-NO (b-1, b-2), and high-NO conditions (c-1, c-2). The upper panels show modeled and measured concentrations of α-pinene, NO, and O_3 across the three conditions, while the lower panels show the corresponding radical concentrations of $RO_2\cdot$ and $HO_2\cdot$. In addition, the lower panels illustrate the relative contributions of $RO_2\cdot + HO_2\cdot$, $RO_2\cdot + RO_2\cdot$ and $RO_2\cdot + NO$ reactions to the total bimolecular reaction rate of $RO_2\cdot$ (shown as $RO_2\cdot$ fate on the right y-axis).

We also updated the conclusions accordingly:

The sum of the major $C_{10}H_{15}O_x\cdot$-related closed-shell HOM products ($C_{10}H_{14}O_x$, $C_{10}H_{15}NO_x$ and $C_{10}H_{16}O_x$) contributes 24% and 34% to the total HOM under low-NO and high-NO conditions, while it is negligible under NO-free conditions.

7. *The extrapolation to Hyytiälä and to megacity conditions should be more carefully framed. Hyytiälä daytime NO is typically well below 0.5 ppbv, whereas the dominant H-abstraction signal here is observed at 7.4 ppbv. A quantitative statement of how the H-abstraction HOM fraction scales between the lab ranges explored and atmospherically relevant NO levels would be valuable and would temper the implied relevance to low-NO boreal conditions.*

Responses:

We thank reviewer for this comment and the suggestion. We agree that direct extrapolation from our chamber conditions to Hyytiälä requires careful consideration and quantitative evaluation. Therefore, in the updated manuscript, we have made several modifications.

1. We performed box model simulations to quantitively estimate $RO_2\cdot$ fates under different experimental conditions, especially regarding the different NO conditions used. Please find the details in our responses to ***Comment 6***.
2. A more detailed comparison between this study and Shen et al. (2022) was extended, which was addressed in our responses to ***Comment 5***.
3. The contribution of H-abstraction to the total HOM formation is now discussed for both high-NO and low-NO conditions, and the corresponding statements in the Abstract and the Conclusions have been revised accordingly, which can be found in our responses to ***Comment 1***.

The application of results observed in our chamber study to the field case (Hyytiälä) was revised accordingly to account for possible uncertainties. The revised part of the Conclusion can be found ***in Comment 1.***

References:

Baker, Y., Kang, S., Wang, H., Wu, R., Xu, J., Zanders, A., He, Q., Hohaus, T., Ziehm, T., Geretti, V., Bannan, T. J., O'Meara, S. P., Voliotis, A., Hallquist, M., McFiggans, G., Zorn, S. R., Wahner, A., and Mentel, T. F.: Impact of HO2⁄RO2 ratio on highly oxygenated α-pinene photooxidation products and secondary organic aerosol formation potential, Atmos. Chem. Phys., 24, 4789-4807, 10.5194/acp-24-4789-2024, 2024.

Berndt, T., Richters, S., Jokinen, T., Hyttinen, N., Kurten, T., Otkjaer, R. V., Kjaergaard, H. G., Stratmann, F., Herrmann, H., Sipila, M., Kulmala, M., and Ehn, M.: Hydroxyl radical-induced formation of highly oxidized organic compounds, NATURE COMMUNICATIONS, 7, 10.1038/ncomms13677, 2016.

Berndt, T.: Peroxy Radical Processes and Product Formation in the OH Radical-Initiated Oxidation of alpha-Pinene for Near-Atmospheric Conditions, J Phys Chem A, 125, 9151-9160, 10.1021/acs.jpca.1c05576, 2021.

Jenkin, M. E., Saunders, S. M., and Pilling, M. J.: The tropospheric degradation of volatile organic compounds: a protocol for mechanism development, Atmospheric Environment, 31, 81-104, https://doi.org/10.1016/S1352-2310(96)00105-7, 1997.

Kang, S., Wildt, J., Pullinen, I., Vereecken, L., Wu, C., Wahner, A., Zorn, S. R., and Mentel, T. F.: Formation of highly oxygenated organic molecules from α-pinene photooxidation: evidence for the importance of highly oxygenated alkoxy radicals, EGUsphere, 2025, 1-33, 10.5194/egusphere-2025-2772, 2025.

Kulmala, M., Kontkanen, J., Junninen, H., Lehtipalo, K., Manninen, H. E., Nieminen, T., Petäjä, T., Sipilä, M., Schobesberger, S., Rantala, P., Franchin, A., Jokinen, T., Järvinen, E., Äijälä, M., Kangasluoma, J., Hakala, J., Aalto, P. P., Paasonen, P., Mikkilä, J., Vanhanen, J., Aalto, J., Hakola, H., Makkonen, U., Ruuskanen, T., Mauldin, R. L., Duplissy, J., Vehkamäki, H., Bäck, J., Kortelainen, A., Riipinen, I., Kurtén, T., Johnston, M. V., Smith, J. N., Ehn, M., Mentel, T. F., Lehtinen, K. E. J., Laaksonen, A., Kerminen, V.-M., and Worsnop, D. R.: Direct Observations of Atmospheric Aerosol Nucleation, Science, 339, 943-946, 10.1126/science.1227385, 2013.

Mauldin, R. L., Tanner, D. J., Heath, J. A., Huebert, B. J., and Eisele, F. L.: Observations of H2SO4and MSA during PEM-Tropics-A, Journal of Geophysical Research: Atmospheres, 104, 5801-5816, 10.1029/98jd02612, 1999.

Shen, H., Vereecken, L., Kang, S., Pullinen, I., Fuchs, H., Zhao, D., and Mentel, T. F.: Unexpected significance of a minor reaction pathway in daytime formation of biogenic highly oxygenated organic compounds, Science Advances, 8, eabp8702, doi:10.1126/sciadv.abp8702, 2022.

Xu, L., Moller, K. H., Crounse, J. D., Otkjaer, R. V., Kjaergaard, H. G., and Wennberg, P. O.: Unimolecular Reactions of Peroxy Radicals Formed in the Oxidation of alpha-Pinene and beta-Pinene by Hydroxyl Radicals, J Phys Chem A, 123, 1661-1674, 10.1021/acs.jpca.8b11726, 2019.

Reviewer 2

Summary

This study explores HOM formation via the H-abstraction pathway of alpha-pinene OH-oxidation by conducting photo-oxidation experiments of alpha-pinene and pinonaldehyde in the SAPHIR-STAR chamber at varying NO levels using H2O2 as an oxidant precursor. This work is novel as it explores another possible source for H-abstraction HOM-RO2 and subsequent products (i.e. pinonaldehyde OH-oxidation). Using two types of chemical ionization techniques and fuzzy c-means clustering, this study finds that fractional contribution of H-abstraction HOM-RO2 and subsequent termination products to total HOM increased with increasing NO.

It's my determination that this work is both within the scope of this journal and the results from these experiments can prove beneficial to the field. However, I have some concerns about the analysis of the data, and I believe some deeper analysis could increase the novelty of the work. Therefore, I recommend reconsidering this manuscript after major revisions.

Major comments

1. *Regarding the experimental setup, a focus is placed on the no NO case having no NO. However, is there no NO or is the level of NO below the limit of detection of your instrument? No LOD is given, and, as shown in the Shen 2022 paper, an off-gassing of HONO from chamber walls could delay a NO reaction with the initial H-abstraction RO2 (C10H15O2) resulting in a delay of isomerization and subsequent HOM-RO2 formation. I have a similar comment with the O3 measurement. What is the LOD and what is the O3 production during the "early reaction stage" (this can be estimated with some 0D box modeling, see below)?*

Responses:

We thank the reviewer for his thoughtful review of our manuscript and for this comment. We agree that the detection limits of NO and O_3 are particularly important, especially in the early reaction stages. The detection limits of NO and O_3 are 0.05 ppb and 0.2 ppb, respectively. Additionally, it should be mentioned that the chamber used in this study is made from glass (Baker et al., 2024) and will not outgas HONO.

These detection limits do not affect our definition of early reaction stage periods, or the subsequent analysis. For example, during the early reaction stages, O_3 production was generally less than 1 ppbv. Therefore, the loss of α-pinene via O_3 oxidation was negligible compared to OH oxidation. We have now added information about the limits of detection to the instrumentation section.

Gas concentrations of NO and NO_x were detected by a NO monitor (nCLD 899, Eco Physics GmbH) coupled to a self-built photolytic NO_2 converter, with a detection limit of 0.05 ppb for NO measurement. The O_3 was measured by an O_3 monitor (O342e, Envea GmbH), with a detection limit of 0.2 ppb.

2. *The authors discussion identifying the "early reaction stage" is unclear to me since the reasoning is not quantitative. This could be limiting their analysis by comparing across the experiments at different extents of reaction. Because they measure many key compounds that affect RO2 and VOC fate, such as NO, HO2, OH, and O3, I recommend some RO2 parameterization and reaction modeling be included in this study to enhance their discussion of RO2 fate and FCM analysis by quantifying the "early reaction stage".*

Responses:

We also thank the reviewer for the suggestion to use box model simulations to estimate the concentrations of $RO_2\cdot$, $HO_2\cdot$, and ·OH, thereby providing a more quantitative definition of the early reaction stage period.

Accordingly, we have performed additional box model simulations for the α-pinene photooxidation experiments, with the chemical mechanistic information based on the Master Chemical Mechanism, MCM v3.3.1 (Jenkin et al., 1997; Saunders et al., 2003). The results were added to Section 2.2: "Model Simulations to Determine Early Reaction Stages" of the manuscript. The relevant diagrams are shown now in Figure 2.

Based on the results of these simulations, the early reaction stage periods are now identified by the $RO_2\cdot$ fate and the loss of α-pinene and pinonaldehyde. In summary, we define the early reaction stages by using three criteria: (i) α-pinene turnover exceeds that of pinonaldehyde by a factor of ten, (ii) under conditions with NO, biomolecular reactions of $RO_2\cdot$ are dominated by $RO_2\cdot$ + NO, contributing more than 90% to $RO_2\cdot$ biomolecular losses, (iii) α-pinene oxidation is primarily driven by ·OH rather than O_3.

However, the determination of early reaction stages by using these box model simulations does not show significant change because previously we had already considered the influence of the RO_2 fate, O_3 reactions, and pinonaldehyde by using less refined model simulations. Previously, early reaction stages were identified within 100 seconds, 100 seconds, and 300 seconds for NO-free, low-NO, and high-NO conditions, respectively. The updated version only changes the length of the period for high-NO conditions to 320 seconds, while time periods for NO-free and low-NO conditions stay the same with 100 seconds.

The newly added Section 2.2: "Model Simulations to Determine Early Reaction Stages" and the updated and added figures in the manuscript and the supplemental material are shown below:

Model simulations to determine early reaction stages

To clarify the role of the H-abstraction channel under varying NO conditions the early reaction stages are particularly relevant. In this study, we define early reaction stages using three criteria: (i) α-pinene turnover exceeds that of pinonaldehyde by a factor of ten, (ii) under conditions with NO, biomolecular reactions of RO_2· are dominated by RO_2· + NO and contribute more than 90% to the biomolecular loss of RO_2·, and (iii) α-pinene oxidation is primarily driven by ·OH rather than O_3. Therefore, model simulations for α-pinene photooxidation systems were conducted to quantitively identify these early reaction stages.

As shown in ***Figure 2 (a-1) to (c-1)***, the model captures the evolution of the system quite well but generally underestimates NO and O_3 concentrations. These discrepancies may arise from differences in the temporal resolution of measurements and simulations, physical effects introduced by the activation of the UVC lamps (e.g., changing emissions due to temperature adjustment of the UVC lamp), and uncertainties in the chemical mechanism including reactions currently not represented in the model framework. The HO_2· and RO_2· concentrations obtained from the simulations are shown in ***Figure 2 (a-2) to (c-2)*** together with the relative contributions of RO_2· + NO, RO_2· + HO_2· and RO_2· + NO to the total biomolecular RO_2 loss. Here, the reaction rates were calculated with $k_{[RO2][HO2]} = 1.85 \cdot 10^{-11}$ cm^3 s^{-1}, $k_{[RO2][NO]} = 1 \cdot 10^{-11}$ cm^3 s^{-1} and $k_{[RO2][RO2]} = 5 \cdot 10^{-12}$ cm^3 s^{-1} (Baker et al., 2024; Berndt et al., 2016; Jenkin et al., 1997).

Based on these results, reactions occurring within the first 100 s, 100 s, and 320 s after initiation of reactions by starting the photooxidation were defined as early stages for the NO-free, low-NO, and high-NO conditions, respectively. The average bimolecular reaction rates for RO_2· + NO were negligible for cases without NO and increased to 0.179 s^{-1} and 1.06 s^{-1} for the low-NO and high-NO conditions, respectively. For RO_2· + HO_2· reactions, the rates were 0.0055 s^{-1}, 0.011 s^{-1}, and 0.0075 s^{-1}, while those for RO_2· + RO_2· reactions were 0.0075 s^{-1}, 0.0029 s^{-1}, and 0.0014 s^{-1} for NO-free, low-NO, and high-NO conditions, respectively. The contribution of RO_2· + NO was higher than 90% under both low-NO and high-NO conditions.

For pinonaldehyde photooxidation under high-NO conditions, the reactions within the early reaction stages were also investigated to facilitate comparison with the corresponding α-pinene system under high NO conditions. Besides H-abstraction channel, reactions of α-pinene with O_3, and pinonaldehyde with ·OH may also contribute to the formation of $C_{10}H_{15}O_x$ radicals. Therefore, the loss of α-pinene due to oxidation by O_3 formed as a byproduct of other reactions, and the loss of pinonaldehyde via ·OH oxidation, were evaluated. The results are shown in detail in ***Figure S5***. In both cases, losses are smaller than 10% of the reaction rate of α-pinene with ·OH, which further supports our definition of early reaction stage being reasonable and representative.

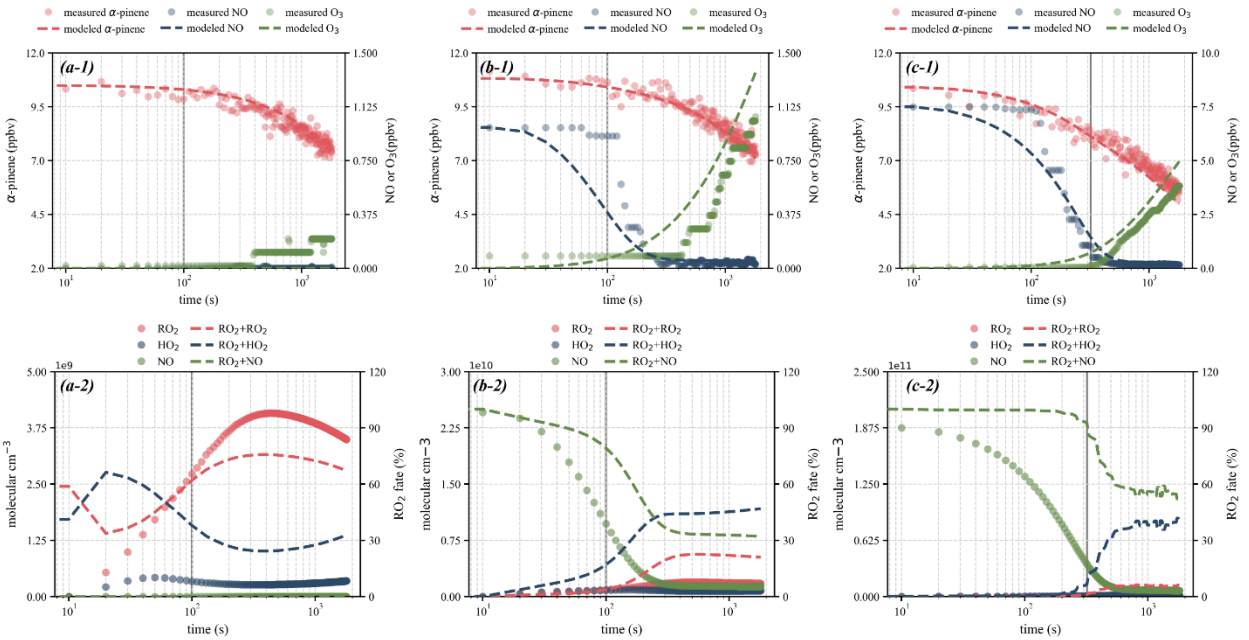

Figure 2. Results of model simulations for α-pinene photooxidation under NO-free (a-1, a-2), low-NO (b-1, b-2), and high-NO conditions (c-1, c-2). The upper panels show modeled and measured concentrations of α-pinene, NO, and O_3 across the three conditions, while the lower panels show the corresponding radical concentrations of RO_2· and HO_2·. In addition, the lower panels illustrate the relative contributions of RO_2· + HO_2·, RO_2· + RO_2· and RO_2· + NO reactions to the total bimolecular reaction rate of RO_2· (shown as RO_2· fate on the right y-axis).

Figure S5 was added to the supplemental information:

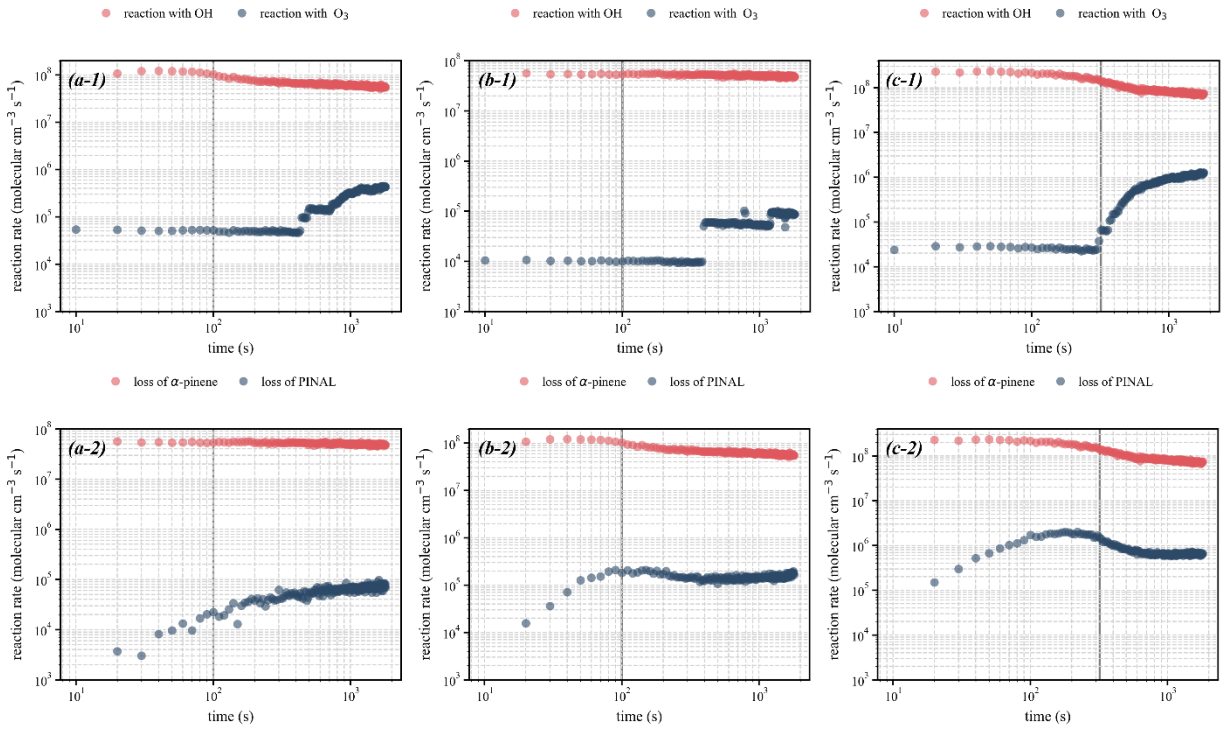

Figure S5. The upper panels (a-1 to c-1) compare the oxidation rates of α-pinene by ·OH and O_3 under NO-free, low-NO, and high-NO conditions, respectively. In each case, the relative contributions of OH- and O_3-initiated oxidation are shown. The lower panels (b-1 to c-1) compare the OH-initiated reaction losses of α-pinene and pinonaldehyde.

Since the time period for early reaction stages for the high-NO condition was slightly adjusted, the previous Figure 2 (now Figure 3) has been updated accordingly. Nevertheless, the overall trends and conclusions remain the same, and no significant differences to the previous version can be observed.

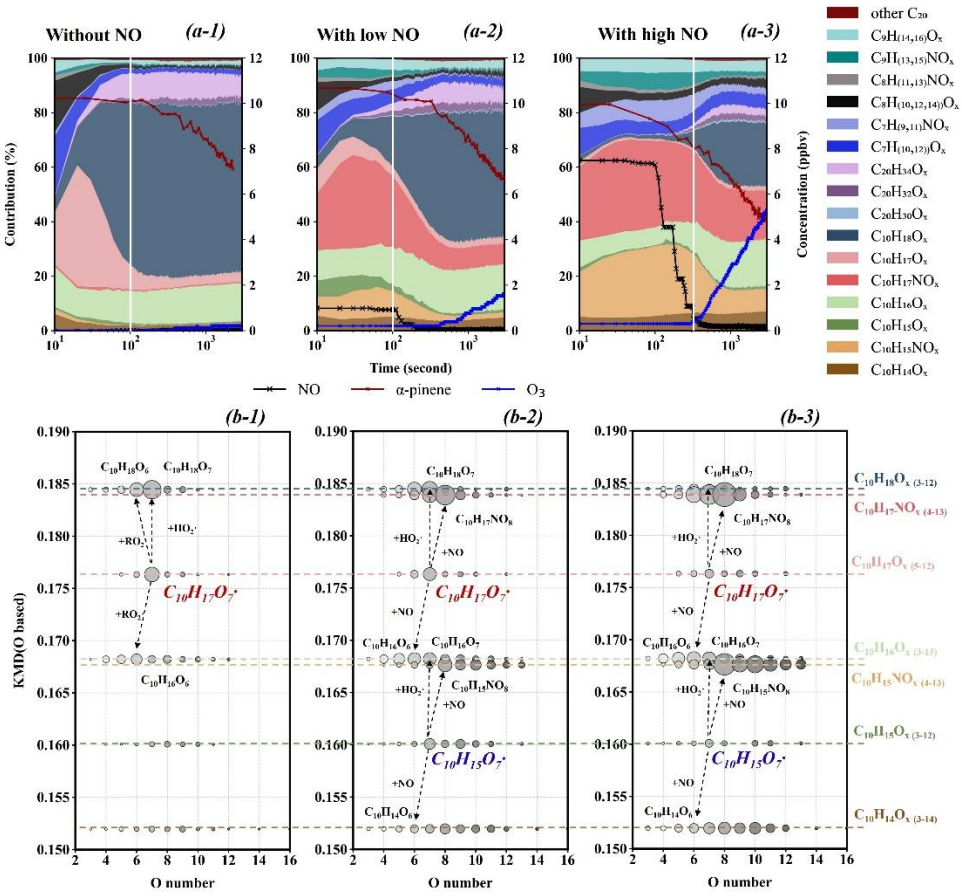

Figure 3. Panels (***a-1, a-2, a-3***) show stacked figures with the contributions of each product family from α-pinene photooxidation as a function of reaction time. The families representing major monomers (C = 10), fragments (C < 10), and accretion products (C = 20) are included in panels ***(a-1, a-2, a-3)***. Time series of concentrations for α-pinene, NO, and O_3 are also presented. The corresponding panels ***(b-1, b-2, b-3)*** located below each stack plot show the Kendrik Mass Defect (KMD, based on oxygen weight) of monomer compounds as a function of oxygen number, with marker sizes indicating the relative abundance of each compound in the early reaction stages (0-100s, 0-100s, and 0-320s after reaction starts for b-1, b-2, and b-3, respectively. This is also indicated by the vertical white lines in a-1, a-2, and a-3). Compounds aligned along the same horizontal dashed lines are in same family, with the same carbon and hydrogen number but differing in oxygen number. Family names are shown on the right. The texts in panels ***(b-1, b-2, b-3)*** highlight major compounds with high abundance and their possible formation pathways. NO conditions increase in the panels from left to right, from NO-free and low-NO to high-NO, respectively. The products here are detected by nitrate-CIMS.

3. A more robust decision could be made by choosing the OH exposure (or reaction time), at which the authors identify a range for "early reaction stage" via some 0D box modeling to quantify pinonaldehyde loss with respect to alpha-pinene loss and relative alpha-pinene loss with respect to O3 oxidation compared to OH oxidation By doing so, the authors will make the discussion in section 3 and statements such as in line 333 ("C10H15O3•, which cannot arise from ozonolysis of α-pinene since O3 formation is negligible in the early reaction stages") more convincing. Finally, because all relevant species are directly measured and calibrated, more quantitative parameters of the RO2 fate could be calculated instead of just estimating the ratio of RO2 reactivity towards NO or HO2.

Responses:

We thank the reviewer for this valuable comment and agree again that model simulations can provide a more quantitative definition of the early reaction stages and strengthen the results. As mentioned before, we have performed additional box-model simulations. The simulations successfully reproduced the observed decay of α-pinene and provided better estimates of the concentrations of the key radicals, including ·OH, RO_2·, and HO_2·.

Using these simulated radical concentrations, we have further evaluated the bimolecular loss pathways of RO_2· radicals, including reactions with HO_2·, NO, and other RO_2· radicals. Details of these calculations are provided in our response to Comment 2.

In addition, we compared the reaction rates of α-pinene with ·OH and O_3 to identify time periods, during which OH-initiated oxidation dominated while O_3-initiated oxidation was negligible. This analysis provides a more quantitative basis for defining the early reaction stages, and supports the results presented in the revised manuscript.

Besides the changes made which have been mentioned in Comment 2, we also revise the discussion part:

The initial peroxy radicals that led to the $C_{10}H_{15}O_x$· related products were identified as $C_{10}H_{15}O_3$·. However, $C_{10}H_{15}O_3$· cannot be the result of ozonolysis of α-pinene since α-pinene was predominantly oxidized by ·OH radicals rather than O_3, as shown in ***Figure S7***.

4. I find discussion used to prove the C10H14Ox compounds come from alpha-pinene H-abstraction instead of pinonaldehyde OH addition unclear. The main issue I have is with the paragraph starting on line 405. First, it is unclear what exactly is being plotted in Figure 4b: the integrated ncps over the course of the experiments or the signal of each species recorded at a similar time. Either way, there is limited discussion on whether [OH]ss or VOC reactivity drives the difference in turnover between alpha-pinene and pinonaldehyde. The loss of closed shell species to OH oxidation could muddle the conclusions here and is not discussed at all. That being said, I think the evidence presented in the

paragraph starting at line 429 is the most convincing and robust and should be highlighted more in this discussion and throughout the paper.

Responses:

We thank the reviewer for this valuable suggestion. We agree that normalizing product signals by the pinonaldehyde turnover in each experiment provides a more appropriate basis for evaluating the contribution of pinonaldehyde oxidation to the formation of C10H15Ox-related HOMs observed during α-pinene oxidation. Accordingly, we have made the following revisions:

1. In addition to the previously mentioned box model simulations, we have substantially revised figure 5 (previously Figure 4). The original Figure 4 was intended to compare product distributions between α-pinene and pinonaldehyde experiments, and to assess whether pinonaldehyde oxidation could explain the observed C10H15Ox-related HOMs in α-pinene photooxidation. In the original Figure 4 the pinonaldehyde turnover was not explicitly quantified since we also did not quantify the concentrations of pinonaldehyde. We agree with the reviewer that the description of Figure 4b was insufficient, and that the definition of the "early reaction stage" was not adequately explained and justified. Therefore, we have revised the Figure. The new Figure 5b now presents product distributions averaged over the early reaction stage periods and normalized to the pinonaldehyde turnover ratio between the two experiments.
2. We also appreciate the reviewer's observations that the discussion about the comparison between α-pinene and pinonaldehyde experiments are important and convincing to highlight the importance of H-abstraction chemistry. Therefore, we have expanded the discussion in the manuscript to clarify the normalization procedure and to explicitly account for differences in ·OH exposure and precursor reactivity when evaluating the role of pinonaldehyde oxidation in forming C10H15Ox-related HOMs. We have also emphasized this evidence in both the Abstract and the Conclusions section.

The following text was added to the manuscript, and Figure 5 was updated as shown below:

To assess the potential contribution of pinonaldehyde oxidation to the formation of $C_{10}H_{15}O_x$·-related HOM, pinonaldehyde photooxidation experiments were conducted under NO-free and high-NO conditions, analogous to conditions applied in the α-pinene systems (***Table 1***). Time series of α-pinene and its oxidation product pinonaldehyde during the first 30 min of the α-pinene (high-NO) experiment are shown in Figure ***5(a-1).*** The corresponding turnovers of α-pinene and pinonaldehyde are presented in Figure ***5(a-1).*** Similarly, the concentration of pinonaldehyde and its turnover during the pinonaldehyde (high-NO) experiment are shown in Figure ***5(a-2).*** ·OH concentrations were estimated using model simulations.

During early stage, the average pinonaldehyde turnover was 8.9×10^6 molecules cm^{-3} s^{-1} under pinonaldehyde (high-NO) condition, approximately 6 times higher than the turnover (1.5×10^6 molecules cm^{-3} s^{-1}) under α-pinene (high-NO) condition. To facilitate comparison between the two experiments, we

calculated the pinonaldehyde turnover for both experiments and compared it to obtain the ratio between the high-NO α-pinene and pinonaldehyde experiment (hereafter referred to as the pinonaldehyde turnover ratio). Signals measured in the pinonaldehyde experiment were subsequently normalized by this ratio to account for differences in the pinonaldehyde turnover between the two experimental systems. The distributions of major $C_{10}H_{15}O_x$·-related products observed during the high-NO α-pinene and high-NO pinonaldehyde experiments are presented in Figure 5(b). Major products belonging to the $C_{10}H_{14}O_x$ and $C_{10}H_{15}NO_x$ family detected by both nitrate-CIMS (N) and amine-CIMS (A) are included. The data shown in ***Figure 5(b)*** represents averages over the first 320 s following the initiation of oxidation, corresponding to the early reaction stage, during which RO_2· + NO accounts for more than 90% of the total bimolecular RO_2· loss rate. In addition, all product signals here as well as all data used for comparison in the following paragraphs have been normalized by the pinonaldehyde turnover.

The pinonaldehyde turnover ratio during the first 320 s exceeded 5 and was substantially higher during the first 100 s. This large difference arises because pinonaldehyde was present at the start of the pinonaldehyde high-NO experiment and was therefore immediately available for reaction with ·OH. In contrast, under α-pinene high-NO conditions, pinonaldehyde had to be formed through α-pinene oxidation before it could undergo further reactions, resulting in a much lower pinonaldehyde turnover during the early stages of the experiment. For $C_{10}H_{15}O_x$·-related HOM detected by nitrate-CIMS the summed signals of the $C_{10}H_{14}O_x$ and $C_{10}H_{15}NO_x$ families under α-pinene high-NO conditions exceed those of pinonaldehyde high-NO conditions by factors of approximately 20 and 10, respectively. Although pinonaldehyde oxidation contributes to the formation of $C_{10}H_{15}O_x$·-related HOM under high-NO conditions, this contribution is minor and can explain approximately 5% of the HOM yield observed from α-pinene oxidation. Similarly, for less oxygenated products measured by amine-CIMS, the summed concentrations of the $C_{10}H_{14}O_x$ and $C_{10}H_{15}NO_x$ families were 98 times higher in the α-pinene high-NO experiment, and 6.7 times higher in the pinonaldehyde high-NO experiment.

For highly oxygenated compounds detected by nitrate-CIMS, species containing more than 10 oxygen atoms account for 11% of the $C_{10}H_{14}O_x$ family and for 13% of the $C_{10}H_{15}NO_x$ family under α-pinene high-NO condition, whereas their contributions are much lower for pinonaldehyde high-NO conditions (3% and 5%, respectively).

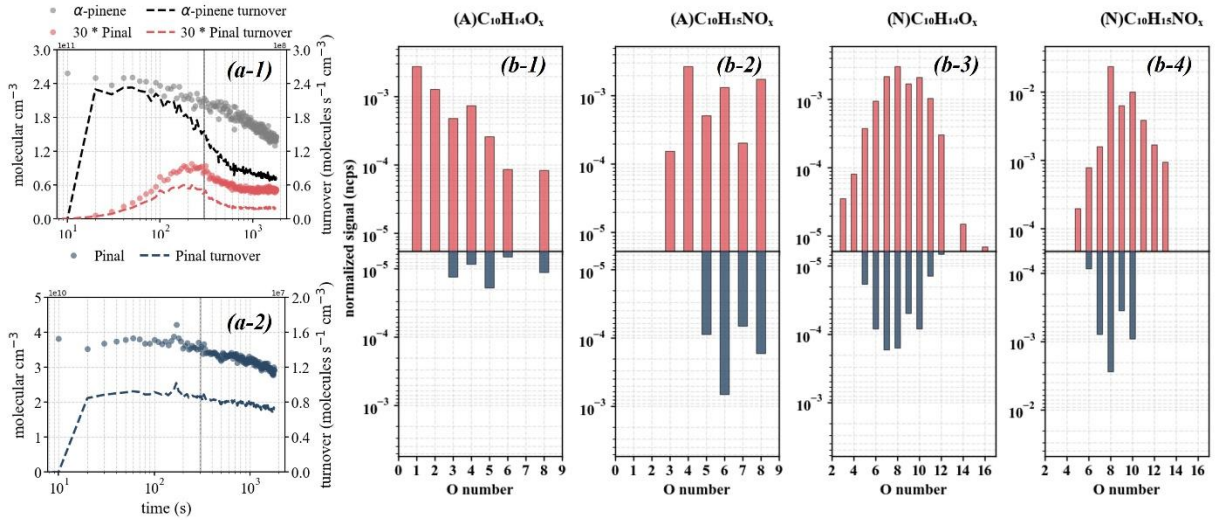

Figure 5. Panel (a-1) displays concentrations and turnover of α-pinene and pinonaldehyde (Pinal) during α-pinene photooxidation under high-NO conditions, while panel (a-2) represents concentrations and turnover of pinonaldehyde during the high-NO pinonaldehyde photooxidation experiment. Major product distributions are shown in panel (b-1) to (b-4). Signals detected in the pinonaldehyde experiment are normalized by the ratio of the pinonaldehyde turnover during the pinonaldehyde experiment to the respective turnover during the α-pinene experiment. The products are separated into four groups: (A)$C_{10}H_{14}O_x$, (A)$C_{10}H_{15}NO_x$, (N)$C_{10}H_{14}O_x$, (N)$C_{10}H_{15}NO_x$, of which (A) and (N) represent signals derived from amine-CIMS and nitrate-CIMS, respectively. Data from α-pinene oxidation and pinonaldehyde oxidation are colored in pink and blue, respectively.

The revised abstract and conclusion are attached below:

Abstract:

Highly oxygenated organic molecules (HOM) are efficiently formed via autooxidation during ·OH-initiated oxidation of α-pinene. We investigated the relative contributions of ·OH-addition and hydrogen (H)-abstraction to HOM formation from α-pinene photooxidation under varying NO conditions. HOM molecules were detected by a nitrate chemical ionization mass spectrometer (CIMS). In the absence of NO, $C_{10}H_{17}O_x$· peroxy radicals and related termination products (e.g. $C_{10}H_{18}O_x$) dominated the HOM spectrum, accounting for more than 70% of total HOM. The presence of NO substantially altered HOM products, particularly by the rapid formation of $C_{10}H_{15}O_x$·-related HOM like $C_{10}H_{15}NO_8$. The ratio of $C_{10}H_{15}NO_x$ to $C_{10}H_{17}NO_x$ increased significantly from 0.34 to 0.84 as the RO_2· loss rate via reaction with NO increased from 0.18 s^{-1} to 1.06 s^{-1}. Under high-NO conditions, $C_{10}H_{15}O_x$·-related HOM contributed up to 34% to total HOM from α-pinene oxidation systems. H-abstraction channel was proven to be the source of $C_{10}H_{15}O_x$·-related HOM. Fuzzy c-means clustering indicated that $C_{10}H_{15}O_x$·-related HOM exhibited the fastest formation rate among the identified HOM groups, consistent with first-generation products. Comparison with pinonaldehyde oxidation, obtained by normalizing HOM yields to pinonaldehyde

turnover, suggests that pinonaldehyde contributed ~5% of HOM in α-pinene systems, excluding secondary oxidation as the dominant source. Detection of $C_{10}H_{15}NO_4$ under high-NO conditions by propylamine-CIMS is indicator for formation of $C_{10}H_{15}O_3\cdot$ peroxy radicals, formed by alkoxy radical decomposition and six-membered ring opening in H-abstraction channel. This study highlights the role of the H-abstraction pathway in OH-initiated α-pinene oxidation under NO-influenced conditions and provides new constraints on detailed HOM formation mechanisms.

Conclusion:

To constrain the potential contribution of H-abstraction to HOM formation, regimes with and without NO were directly compared, and a separate experiment of pinonaldehyde oxidation under similar conditions was performed. Additionally, measurements by Amine-CIMS were used to detect less oxygenated products. Since the photolysis of H_2O_2 was utilized to produce ·OH radicals O_3 did not accumulate during the early reaction stages; therefore, ozonolysis did not interfere with the ·OH pathways. FCM analysis proves that the dominant species in the $C_{10}H_{15}NO_x$ family, $C_{10}H_{15}NO_8$ and $C_7H_9NO_8$, can be distinguished from other species by their fast formation rates in the presence of NO. Pinonaldehyde oxidation can only contribute ~ 5% to HOM formation in α-pinene oxidation systems. Therefore, neither ozonolysis nor secondary oxidation can explain the significant formation of $C_{10}H_{15}O_x\cdot$-related HOM, which points to H-abstraction from α-pinene by ·OH being the most likely formation pathway.

As illustrated in ***Figure S10*** and ***Figure S11,*** the contribution of the H-abstraction pathway to HOM formation increases with elevated NO levels compared to the ·OH addition pathway. The ratios between major $C_{10}H_{15}O_x\cdot$-related HOM and $C_{10}H_{17}Ox\cdot$-related HOM rise with increasing NO concentrations. The ratio of $C_{10}H_{15}O_x\cdot$ peroxy radicals to $C_{10}H_{17}O_x\cdot$ peroxy radicals is 0.06, 0.83, and 1.42 under NO-free, low-NO, and high-NO conditions, respectively. Similarly, the ratio of $C_{10}H_{15}NO_x$ to $C_{10}H_{17}NO_x$ increases from 0.34 to 0.84 when NO levels increase from low to high. The sum of the major $C_{10}H_{15}O_x\cdot$-related closed-shell HOM products ($C_{10}H_{14}O_x$, $C_{10}H_{15}NO_x$ and $C_{10}H_{16}O_x$) contributes 24% and 34% to the total HOM under low-NO and high-NO conditions, while it is negligible under NO-free conditions.

Minor comments

Throughout the figures (Fig 2a, Fig 4a), the NO measurements look stepwise. What was the frequency of data acquisition? Were these points interpolated?

Response:

We thank the reviewer for this comment. The NO monitor acquires a new sample every 45 seconds, which explains the stepwise appearance of the NO in the figures. To compare the NO data with other measurements (e.g., CIMS and PTR data) and model simulations, the NO data was interpolated onto a 10

second grid for consistent temporal alignment. We note that this interpolation does not introduce additional information and only provides a temporally consistent representation for the analysis.

Line 58: It is unclear what is meant by "the latter," as the comparison in the previous paragraph was OH-addition vs OH-abstraction, but C10H17O3• don't form via OH-abstraction.

Response:

We thank the reviewer for mentioning this. We have significantly revised this paragraph to make it clearer:

α-pinene is globally the most abundant monoterpene and has been shown to form significant amounts of HOM when it is oxidized by O_3 or by hydroxyl radical (·OH) (Ehn et al., 2014; Berndt et al., 2016). ·OH initiated oxidation of α-pinene occurs via the OH-addition pathway (~90%) and the hydrogen (H)-abstraction pathway (~10%), leading to the formation of peroxy radicals (RO_2·) with the formulas $C_{10}H_{17}O_3$· and $C_{10}H_{15}O_2$·, respectively (Vereecken et al., 2007).

Line 70: Vereecken et al. (2007) has only a limited discussion of the H-abstraction pathway of alpha-pinene oxidation and only specifically comments on later generation fragmentation products of the H-abstraction pathway in the atmosphere vs the chamber (see figures 3+4).

Response:

We thank the reviewer for this comment. We agree that Vereecken et al. (2007) only provide a limited discussion of the H-abstraction pathway and is not directly appropriate for supporting this statement. We have therefore removed this citation and revised the sentence accordingly:

The detection of $C_{10}H_{15}O_x$ related products with fewer than five oxygen atoms suggests contributions from H-abstraction pathways

Line 181: Grammatical error.

Response:

We thank the reviewer for pointing this error out. We have revised this sentence as follows:

The concentration of ·OH radicals was calculated based on the reacted fraction of α-pinene or pinonaldehyde under steady-state conditions (**Eq.1**) (Kiendler-Scharr et al., 2009). When the system is in steady-state, all parameters are stable and injection rates equal loss rates.

Line 232: "Under no-NO" is formatted awkwardly surrounding the table.

Response:

We thank the reviewer for pointing this error out. We revised this sentence and also changed no-NO to NO-free or "without NO" throughout the manuscript:

Under α-pinene photooxidation conditions without NO, …

Lines 243-249: There is a paragraph break contains multiple ideas. It's a bit hard to follow clearly.

Response:

We thank the reviewer for this comment, and we agree with reviewer that the previous version was difficult to understand. Therefore, we revised this part to:

Compounds with six oxygen atoms but one hydrogen less or one more hydrogen (i.e., $C_{10}H_{16}O_6$ and $C_{10}H_{18}O_6$) are significant contributors to the total product signal of the $C_{10}H_{17}O_x\cdot$ family. Compounds with the formula $C_{10}H_{16}O_6$ likely have carbonyl functionalities and are formed either directly from reaction R3 or from self-termination reactions of $C_{10}H_{17}O_7\cdot$ (reaction R8) (Iyer et al., 2018; Jenkin et al., 2019). In contrast, $C_{10}H_{18}O_6$ species are possibly alcohols formed from $C_{10}H_{17}O_7\cdot$ via reaction R3, or more likely hydroperoxides derived from $C_{10}H_{17}O_6\cdot$ via reaction R1 (Iyer et al., 2018; Jenkin et al., 2019).

The following sentence was deleted:

The appearance of compounds with C<10 indicates the formation of alkoxy radicals, since alkoxy radicals can fragment to form species with less than ten carbon atmos.

Line 309: "formula" instead of "formular"

Response:

We that the reviewer for pointing this error out. We replaced formular with 'formula'.

Line 344: Are the KMD plots showing the integrated contribution over the course of the total "early reaction stage" or is it at the top limit?

Response:

We thank the reviewer for this comment. The KMD plots present the average contribution over the entire early-stage reaction period. The related description has been updated:

The average product distributions of C_{10} monomers from early stage α-pinene photooxidation without and with NO are illustrated by Kendrik Mass Defect (KMD) plots as a function of oxygen number (Kendrick Mass = oxygen, ***Figure2 (b-1, b-2, b-3)***).

Line 484: Why would the use of a different type of inlet effect the measurement sensitivity of just one class of HOM? Is there evidence to back up this hypothesis? The experimental conditions and chamber were different between the authors experiments and the Shen et al 2022 experiments. Could that be a reason differences are observed?

Responses:

We thank the reviewer for this comment. We agree that the comparison with Shen et al. (Shen et al., 2022) should be performed with more caution, as the two studies were conducted under different experimental conditions. In the revised manuscript, we have expanded the discussion and now explicitly address several factors that may contribute to the discrepancy, including differences in reaction time, RO_2· fates under high-NO conditions, and instrumental setup.

Although we performed experiments with different ·OH sources, the ·OH level and ·OH exposure are comparable between the two experiments. In our study, more HO_2· radicals were produced due to the reaction between H_2O_2 and ·OH, resulting in an order of magnitude higher HO_2· concentrations compared to Shen et al.'s study (Shen et al., 2022). However, the box model simulations showed that under high-NO conditions the RO_2· + NO reaction rate can explain more than 95% of the biomolecular RO_2· losses, which is consistent with Shen et al. Additionally, only early reaction stages were considered for both studies, during which secondary oxidation was negligible and RO_2· + NO reactions were dominant among RO_2· biomolecular reactions. Therefore, the chemical processes are comparable between the two studies. However, the different chambers could introduce different wall loss rates, which could in turn introduce uncertainty in determining HOM yields and product distributions.

To strengthen the discussion about the different inlets, we now include evidence from a previous inter-comparison measurement designed to evaluate the performance of an Eisele inlet and a MION inlet system. The measurements suggest that the detection efficiency for less-oxygenated HOM (O<8) differs between the two inlet configurations. For example, less-oxygenated C10H17Ox-related HOM were detected with higher efficiency by the MION compared to the Eisele inlet (***Figure S12***). Therefore, the relative contribution of C10H15Ox-related HOM might be higher in the Eisele inlet. Since this study used a MION inlet, whereas Shen et al. (Shen et al., 2022) used an Eisele inlet, inlet-dependent sensitivity differences could partly explain the lower contribution of H-abstraction related products.

We extended the discussion and added one more plot to show the different measurement results between Eisele inlet and MION inlet (Figure S17):

The contribution of H-abstraction related products observed in this study was lower than that reported by Shen and coworkers, who reported a contribution of more than 70% (Shen et al., 2022). The experiments from the two studies were conducted in different chambers, under different conditions and with different instrumentations applied. Two chambers could introduce different wall losses of HOM, which can be further different between less oxygenated HOM and highly oxygenated HOM.

In this study the ·OH radicals were generated via photolysis of H_2O_2, whereas HONO photolysis was the main source of ·OH in Shen et al. (2022). The consecutive reaction between ·OH and H_2O_2 in our experiments leads to an enhanced production of HO_2· radicals, resulting in an HO_2· concentration of ~4×10^8 molecule cm^{-3}, which is approximately one order of magnitude higher than that reported by Shen et al.

(2022). Also, the NO concentration in Shen et al. was constantly around ~20 ppb, while it was only ~7 ppb before reaction in our study, resulting in a concentration of ~1 ppb during the early-reaction stage. Despite these differences, the contributions of RO_2· + NO reactions are dominant in both studies, accounting for more than 95% of RO_2· biomolecular losses under high-NO conditions. In addition, we did only consider early reaction stages, during which secondary oxidation was negligible and RO_2· chemistry was dominated by autoxidation and RO_2· + NO reactions. Therefore, the chemical system can be expected to be similar for both studies, at least under high-NO conditions. However, the constantly higher level of NO in the study by Shen et al. (2022) may continuously promote the H-abstraction channel.

The discrepancy may also arise from differences in measurement techniques: Shen et al. (2022) used an Eisele type inlet (Mauldin et al., 1999), while in this study a MION inlet was used (Rissanen et al., 2019). To compare both inlet systems, we conducted an experiment where both types of inlets were simultaneously used to measure the same oxidation systems. The reference system was α-pinene oxidation by ·OH, with the addition of NO (***Figure S17).*** The results indicate that the MION inlets detects a larger fraction of lesser oxygenated HOM (less than eight oxygen atoms) than the Eisele inlet, and that these HOM dominate the $C_{10}H_{17}O_x$·-related HOM family, while the relative contribution of higher oxygenated HOM (more than eight oxygen atoms) was larger in the study by Shen et al. (2022). When only the highly oxygenated HOM compounds are considered as was done in the study be Shen and coworkers, the relative contribution of $C_{10}H_{15}O_x$·-related HOM to the total HOM does increase to 64%. Therefore, a deeper comparison of the two inlet types may be of interest in the future but is outside the scope of this study.

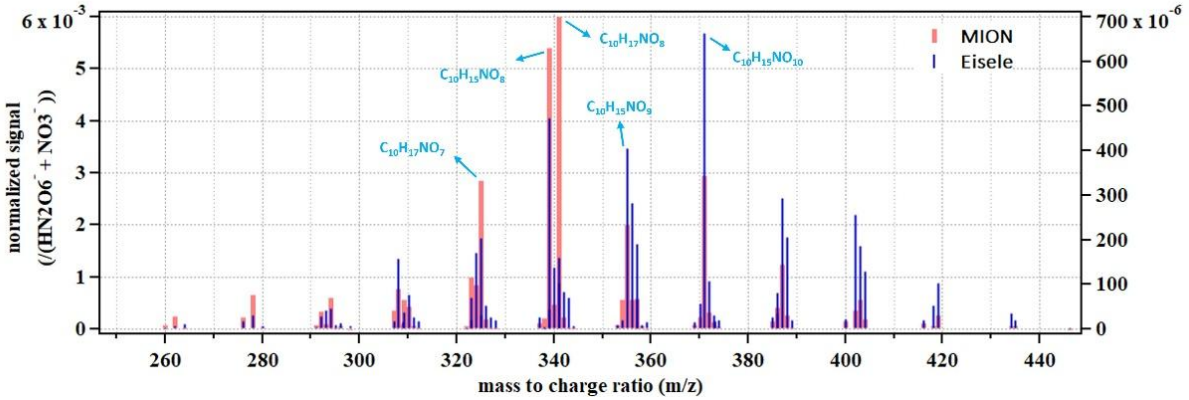

Figure S17. The signal of products derived from α-pinene oxidation with NO injection, detected by CIMS coupled with the MION (pink) and Eisele (blue) inlets.

References:

Baker, Y., Kang, S., Wang, H., Wu, R., Xu, J., Zanders, A., He, Q., Hohaus, T., Ziehm, T., Geretti, V., Bannan, T. J., O'Meara, S. P., Voliotis, A., Hallquist, M., McFiggans, G., Zorn, S. R., Wahner, A., and Mentel, T. F.: Impact of HO2/RO2 ratio on highly oxygenated α-pinene photooxidation products and

secondary organic aerosol formation potential, Atmos. Chem. Phys., 24, 4789-4807, 10.5194/acp-24-4789-2024, 2024.

Berndt, T., Richters, S., Jokinen, T., Hyttinen, N., Kurten, T., Otkjaer, R. V., Kjaergaard, H. G., Stratmann, F., Herrmann, H., Sipila, M., Kulmala, M., and Ehn, M.: Hydroxyl radical-induced formation of highly oxidized organic compounds, NATURE COMMUNICATIONS, 7, 10.1038/ncomms13677, 2016.

Iyer, S., Reiman, H., Moller, K. H., Rissanen, M. P., Kjaergaard, H. G., and Kurten, T.: Computational Investigation of RO(2) + HO(2) and RO(2) + RO(2) Reactions of Monoterpene Derived First-Generation Peroxy Radicals Leading to Radical Recycling, J Phys Chem A, 122, 9542-9552, 10.1021/acs.jpca.8b09241, 2018.

Jenkin, M. E., Saunders, S. M., and Pilling, M. J.: The tropospheric degradation of volatile organic compounds: a protocol for mechanism development, Atmospheric Environment, 31, 81-104, https://doi.org/10.1016/S1352-2310(96)00105-7, 1997.

Jenkin, M. E., Valorso, R., Aumont, B., and Rickard, A. R.: Estimation of rate coefficients and branching ratios for reactions of organic peroxy radicals for use in automated mechanism construction, Atmospheric Chemistry and Physics, 19, 7691-7717, 10.5194/acp-19-7691-2019, 2019.

Kiendler-Scharr, A., Wildt, J., Dal Maso, M., Hohaus, T., Kleist, E., Mentel, T. F., Tillmann, R., Uerlings, R., Schurr, U., and Wahner, A.: New particle formation in forests inhibited by isoprene emissions, Nature, 461, 381-384, 10.1038/nature08292, 2009.

Mauldin, R. L., Tanner, D. J., Heath, J. A., Huebert, B. J., and Eisele, F. L.: Observations of H2SO4and MSA during PEM-Tropics-A, Journal of Geophysical Research: Atmospheres, 104, 5801-5816, 10.1029/98jd02612, 1999.

Saunders, S. M.; Jenkin, M. E.; Derwent, R. G.; Pilling, M. J.: Protocol for the development of the Master Chemical Mechanism, MCM v3 (Part A): tropospheric degradation of non-aromatic volatile organic compounds. Atmos. Chem. Phys. 2003, *3* (1), 161-180. DOI: 10.5194/acp-3-161-2003.

Shen, H., Vereecken, L., Kang, S., Pullinen, I., Fuchs, H., Zhao, D., and Mentel, T. F.: Unexpected significance of a minor reaction pathway in daytime formation of biogenic highly oxygenated organic compounds, Science Advances, 8, eabp8702, doi:10.1126/sciadv.abp8702, 2022.

Vereecken, L., Muller, J. F., and Peeters, J.: Low-volatility poly-oxygenates in the OH-initiated atmospheric oxidation of alpha-pinene: impact of non-traditional peroxyl radical chemistry, Phys Chem Chem Phys, 9, 5241-5248, 10.1039/b708023a, 2007

Wu, R., Zorn, S. R., Kang, S., Kiendler-Scharr, A., Wahner, A., and Mentel, T. F.: Application of fuzzy c-means clustering for analysis of chemical ionization mass spectra: insights into the gas phase chemistry of NO3-initiated oxidation of isoprene, Atmospheric Measurement Techniques, 17, 1811-1835, 10.5194/amt-17-1811-2024, 2024.

Yan, C., Nie, W., Äijälä, M., Rissanen, M. P., Canagaratna, M. R., Massoli, P., Junninen, H., Jokinen, T., Sarnela, N., Häme, S. A. K., Schobesberger, S., Canonaco, F., Yao, L., Prévôt, A. S. H., Petäjä, T., Kulmala, M., Sipilä, M., Worsnop, D. R., and Ehn, M.: Source characterization of highly oxidized multifunctional compounds in a boreal forest environment using positive matrix factorization, Atmospheric Chemistry and Physics, 16, 12715-12731, 10.5194/acp-16-12715-2016, 2016.

Zhang, J., Zhao, J., Luo, Y., Mickwitz, V., Worsnop, D., and Ehn, M.: On the potential use of highly oxygenated organic molecules (HOMs) as indicators for ozone formation sensitivity, Atmospheric Chemistry and Physics, 24, 2885-2911, 10.5194/acp-24-2885-2024, 2024.

Shunyu Yao

Major Comment:

Scientific Significance

I want to raise some concerns regarding the key finding presented in this manuscript, as one major part of the result overlaps significantly with a 2022 Science paper. (Shen et al., 2022) In the previous publication, the effect of NO has already been discussed, and mechanisms have been thoroughly evaluated. This manuscript does show innovation through the no NO condition, which was not present in previous research, and the addition of pinonaldehyde control, which offered a concrete conclusion to the formation pathway. However, the overlap in key conclusions with prior work is substantial. I will list some overlapping parts in conclusion from both the manuscript and publication.

2022 Paper: "the formation rate of C10H15OX•-related HOM is mainly affected by the NO concentration." "In this study, RO• are mainly formed by the alkoxy step (RO2• + NO ➔ RO• + NO2), whose reaction rate depends on the current NO concentration, while the ring opening is especially fast with a typical rate >106 s−1. As a consequence, the formation rate of C10H15OX-related HOM is mainly affected by the NO concentration."

Manuscript conclusion: "C10H15Ox·-related HOM exhibits a strong dependence on NO levels and can only be formed in significant amounts in the presence of NO."

2022 Paper: "time series of C10H17OX•-related HOM are similar at low and high NO."

Manuscript result: "The C10H17O7· peroxy radicals exhibit a rapid formation rate and a high molar yield in α-pinene photooxidation, and the formation is not strongly dependent on NO concentration."

2022 Paper also made a time-based analysis to assess whether pinonaldehyde oxidation will result in C10H15OX formation and ruled out such possibility as pinonaldehyde takes longer to form than H-abstraction product. The manuscript used a similar approach by cluster definition and had the same conclusion.

Pinonaldehyde oxidation control was a novel approach which was not present in the 2022 paper. This control allows readers to directly compare yield of HOM produced from pinonaldehyde oxidation and H-abstraction, in which case H-abstraction had much better yield. This combined with cluster time difference provides stronger evidence of why C10H15Ox does not originate from pinonaldehyde oxidation. There are other novel approaches in this manuscript, such as using both amine-CIMS and nitrate-CIMS to capture a broader range of products, including less-oxygenated species.

The conclusion also addresses one important finding, stating that the contribution of the H-abstraction related products observed in this study is 70 % lower than that reported in the 2022 paper. Authors contributed this difference to inlet, stating that multi-scheme ionization inlet was used for this study, while the 2022 paper used Eisele type inlet. The lower value reported in this manuscript could be an interesting path to pursue, but no direct explanation was given.

The scientific significance would benefit from clearer positioning relative to prior work, particularly the 2022 study. The study applies largely novel experimental approaches to a system whose core conclusions are broadly consistent with prior literature. The scope of detection was widened, and additional control experiments have been done to enhance conclusions. I believe it's an excellent addition to this field of study, but the conclusion does seem to repeat the older paper.

Responses:

We thank Shunyu Yao for his extensive community comment in general and for this thoughtful comment in particular. We agree that the current abstract and conclusion are focusing on the confirmation of the findings reported by Shen et al. (2022), rather than emphasizing the novelty of the present work. The motivation of this work arises from discrepancies between Shen et al. (2022) and other studies (Berndt et al., 2016; Berndt, 2021; Xu et al., 2019), in which the role of the H-abstraction pathway was considered negligible. The objective of this work is not to reproduce the previous results, but to validate and constrain the findings presented in Shen et al. (2022), and to extend the mechanistic understanding of H-abstraction by systematically exploring related experimental conditions in a well-controlled steady-state chamber (Baker et al., 2024).

In this context, the main novelties of the present study are as follows:

1. A fully NO-free condition has been included, allowing a direct comparison between regimes without and with NO presented, which provides stronger constraints on the role of NO for the H-abstraction pathway in HOM formation. NO-free in this study refers to conditions where the measured NO concentration was below the detection limit, in our case below 50 ppt.
2. The combined use of CIMS with nitrate and amine ionization modes enables a broader coverage of the product distributions, particularly of less oxygenated intermediates (e.g., C10H15NO4). In the case α-pinene photooxidation, the H-abstraction channel can result in an opening of the six-membered ring and subsequently to the formation of peroxy radicals, which are potentially linked to the above-mentioned intermediates like C10H15NO4.
3. To constrain the importance of the H-abstraction channel and to deepen the mechanistic understanding, we also conducted pinonaldehyde photooxidation experiments under comparable

conditions as in the α-pinene experiments, which helps to further evaluate the current understanding and to assess the contribution of pinonaldehyde oxidation, a concurrent pathway, to the observed C10H15Ox-related HOM formation in the α-pinene system.

We have therefore revised and extended the manuscript to clarify these points and to better emphasize the new aspects and the constraints provided by the present study, which distinguish it from previous works.

Revised Abstract:

Highly oxygenated organic molecules (HOM) are efficiently formed via autooxidation during ·OH-initiated oxidation of α-pinene. We investigated the relative contributions of ·OH-addition and hydrogen (H)-abstraction to HOM formation from α-pinene photooxidation under varying NO conditions. HOM molecules were detected by a nitrate chemical ionization mass spectrometer (CIMS). In the absence of NO, $C_{10}H_{17}O_x$· peroxy radicals and related termination products (e.g. $C_{10}H_{18}O_x$) dominated the HOM spectrum, accounting for more than 70% of total HOM. The presence of NO substantially altered HOM products, particularly by the rapid formation of $C_{10}H_{15}O_x$·-related HOM like $C_{10}H_{15}NO_8$. The ratio of $C_{10}H_{15}NO_x$ to $C_{10}H_{17}NO_x$ increased significantly from 0.34 to 0.84 as the RO_2· loss rate via reaction with NO increased from 0.18 s^{-1} to 1.06 s^{-1}. Under high-NO conditions, $C_{10}H_{15}O_x$·-related HOM contributed up to 34% to total HOM from α-pinene oxidation systems. H-abstraction channel was proven to be the source of $C_{10}H_{15}O_x$·-related HOM. Fuzzy c-means clustering indicated that $C_{10}H_{15}O_x$·-related HOM exhibited the fastest formation rate among the identified HOM groups, consistent with first-generation products. Comparison with pinonaldehyde oxidation, obtained by normalizing HOM yields to pinonaldehyde turnover, suggests that pinonaldehyde contributed ~5% of HOM in α-pinene systems, excluding secondary oxidation as the dominant source. Detection of $C_{10}H_{15}NO_4$ under high-NO conditions by propylamine-CIMS is indicator for formation of $C_{10}H_{15}O_3$· peroxy radicals, formed by alkoxy radical decomposition and six-membered ring opening in H-abstraction channel. This study highlights the role of the H-abstraction pathway in OH-initiated α-pinene oxidation under NO-influenced conditions and provides new constraints on detailed HOM formation mechanisms.

Revised Conclusions:

In this study a series of photooxidation experiments was conducted under varying NO levels to investigate the effect of NO on the $C_{10}H_{15}O_x$·-related HOM formation in the α-pinene photooxidation system, and to unravel potential formation pathways of these products. The chemical system was brought to a steady state in the dark. Afterwards, reactions were initiated by photolyzing H_2O_2. We focused on early reaction stages (the first hundreds of seconds), during which RO_2· + NO reactions and RO_2· autoxidation reactions dominate the fate of the RO_2·. $C_{10}H_{17}O_x$·-related HOM are dominantly formed via

the ·OH·-addition pathway. Product distributions, potential formation pathways, and rates of $C_{10}H_{17}O_x$·-related HOM have been widely and extensively studied (Berndt, 2021; Xu et al., 2019), and our findings on $C_{10}H_{17}O_x$·-related HOM formation are consistent with previous studies. However, potential formation pathways, distributions, and NO dependence of $C_{10}H_{15}O_x$·-related compounds derived from H-abstraction channel were missing systematic exploration so far.

To constrain the potential contribution of H-abstraction to HOM formation, regimes with and without NO were directly compared, and a separate experiment of pinonaldehyde oxidation under similar conditions was performed. Additionally, measurements by Amine-CIMS were used to detect less oxygenated products. Since the photolysis of H_2O_2 was utilized to produce ·OH radicals O_3 did not accumulate during the early reaction stages; therefore, ozonolysis did not interfere with the ·OH pathways. FCM analysis proves that the dominant species in the $C_{10}H_{15}NO_x$ family, $C_{10}H_{15}NO_8$ and $C_7H_9NO_8$, can be distinguished from other species by their fast formation rates in the presence of NO. Pinonaldehyde oxidation can only contribute ~ 5% to HOM formation in α-pinene oxidation systems. Therefore, neither ozonolysis nor secondary oxidation can explain the significant formation of $C_{10}H_{15}O_x$·-related HOM, which points to H-abstraction from α-pinene by ·OH being the most likely formation pathway.

As illustrated in ***Figure S12*** and ***Figure S15,*** the contribution of the H-abstraction pathway to HOM formation increases with elevated NO levels compared to the OH-addition pathway. The ratios between major $C_{10}H_{15}O_x$·-related HOM and $C_{10}H_{17}Ox$·-related HOM rise with increasing NO concentrations. The ratios of $C_{10}H_{15}O_x$· peroxy radicals to $C_{10}H_{17}O_x$· peroxy radicals are 0.06, 0.83, and 1.42 under NO-free, low-NO, and high-NO conditions, respectively. Similarly, the ratio of $C_{10}H_{15}NO_x$ to $C_{10}H_{17}NO_x$ increases from 0.34 to 0.84 when NO levels increase from low to high. The sum of major $C_{10}H_{15}O_x$·-related closed-shell HOM products ($C_{10}H_{14}O_x$, $C_{10}H_{15}NO_x$ and $C_{10}H_{16}O_x$) contributes 24% and 34% under low-NO and high-NO conditions, while being negligible under NO-free conditions.

The comparison between α-pinene and pinonaldehyde was highlighted:

HOM formation in each system was normalized by the pinonaldehyde turnover and discussion was extended. To calculate the turnover, ·OH radicals were estimated by box model simulations. The revised manuscript was attached as follows:

To assess the potential contribution of pinonaldehyde oxidation to the formation of $C_{10}H_{15}O_x$·-related HOM, pinonaldehyde photooxidation experiments were conducted under NO-free and high-NO conditions, analogous to conditions applied in the α-pinene systems (***Table 1***). Time series of α-pinene and its oxidation product pinonaldehyde during the first 30 min of the α-pinene (high-NO) experiment are shown in Figure ***5(a-1).*** The corresponding turnovers of α-pinene and pinonaldehyde are presented in Figure ***5(a-1).*** Similarly, the concentration of pinonaldehyde and its turnover during the pinonaldehyde

(high-NO) experiment are shown in Figure ***5(a-2).*** ·OH concentrations were estimated using model simulations.

During early stage, the average pinonaldehyde turnover was 8.9 × 10^6 molecules cm^{-3} s^{-1} under pinonaldehyde (high-NO) condition, approximately 6 times higher than the turnover (1.5 × 10^6 molecules cm^{-3} s^{-1}) under α-pinene (high-NO) condition. To facilitate comparison between the two experiments, we calculated the pinonaldehyde turnover for both experiments and compared it to obtain the ratio between the high-NO α-pinene and pinonaldehyde experiment (hereafter referred to as the pinonaldehyde turnover ratio). Signals measured in the pinonaldehyde experiment were subsequently normalized by this ratio to account for differences in the pinonaldehyde turnover between the two experimental systems. The distributions of major $C_{10}H_{15}O_x$·-related products observed during the high-NO α-pinene and high-NO pinonaldehyde experiments are presented in Figure 5(b). Major products belonging to the $C_{10}H_{14}O_x$ and $C_{10}H_{15}NO_x$ family detected by both nitrate-CIMS (N) and amine-CIMS (A) are included. The data shown in ***Figure 5(b)*** represents averages over the first 320 s following the initiation of oxidation, corresponding to the early reaction stage, during which RO_2· + NO accounts for more than 90% of the total bimolecular RO_2· loss rate. In addition, all product signals here as well as all data used for comparison in the following paragraphs have been normalized by the pinonaldehyde turnover.

The pinonaldehyde turnover ratio during the first 320 s exceeded 5 and was substantially higher during the first 100 s. This large difference arises because pinonaldehyde was present at the start of the pinonaldehyde high-NO experiment and was therefore immediately available for reaction with ·OH. In contrast, under α-pinene high-NO conditions, pinonaldehyde had to be formed through α-pinene oxidation before it could undergo further reactions, resulting in a much lower pinonaldehyde turnover during the early stages of the experiment. For $C_{10}H_{15}O_x$·-related HOM detected by nitrate-CIMS the summed signals of the $C_{10}H_{14}O_x$ and $C_{10}H_{15}NO_x$ families under α-pinene high-NO conditions exceed those of pinonaldehyde high-NO conditions by factors of approximately 20 and 10, respectively. Although pinonaldehyde oxidation contributes to the formation of $C_{10}H_{15}O_x$·-related HOM under high-NO conditions, this contribution is minor and can explain approximately 5% of the HOM yield observed from α-pinene oxidation. Similarly, for less oxygenated products measured by amine-CIMS, the summed concentrations of the $C_{10}H_{14}O_x$ and $C_{10}H_{15}NO_x$ families were 98 times higher in the α-pinene high-NO experiment, and 6.7 times higher in the pinonaldehyde high-NO experiment.

For highly oxygenated compounds detected by nitrate-CIMS, species containing more than 10 oxygen atoms account for 11% of the $C_{10}H_{14}O_x$ family and for 13% of the $C_{10}H_{15}NO_x$ family under α-pinene high-NO condition, whereas their contributions are much lower for pinonaldehyde high-NO conditions (3% and 5%, respectively).

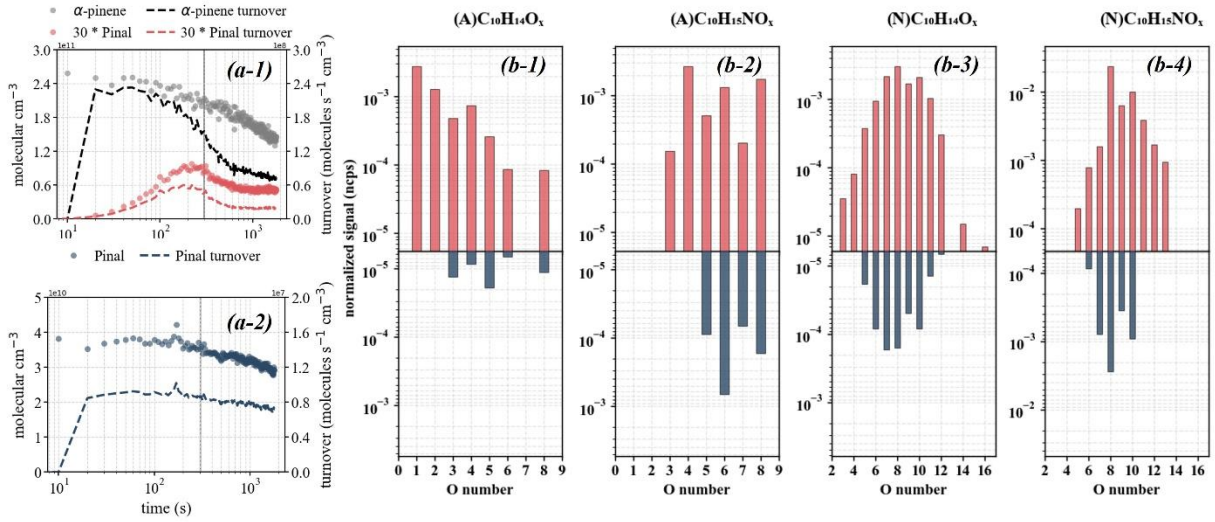

Figure 5. Panel (a-1) displays concentrations and turnover of α-pinene and pinonaldehyde (Pinal) during α-pinene photooxidation under high-NO conditions, while panel (a-2) represents concentrations and turnover of pinonaldehyde during the high-NO pinonaldehyde photooxidation experiment. Major product distributions are shown in panel (b-1) to (b-4). Signals detected in the pinonaldehyde experiment are normalized by the ratio of the pinonaldehyde turnover during the pinonaldehyde experiment to the respective turnover during the α-pinene experiment. The products are separated into four groups: (A)$C_{10}H_{14}O_x$, (A)$C_{10}H_{15}NO_x$, (N)$C_{10}H_{14}O_x$, (N)$C_{10}H_{15}NO_x$, of which (A) and (N) represent signals derived from amine-CIMS and nitrate-CIMS, respectively. Data from α-pinene oxidation and pinonaldehyde oxidation are colored in pink and blue, respectively.

We added a discussion about the reason why we observed a lower contribution of H-abstraction to total HOM formation (~30%) than the contribution from Shen et al., (2022) where they gained a contribution of up to 70%.

In the revised manuscript, we have expanded the discussion and now explicitly address several factors that may contribute to the discrepancy, including differences in reaction time, RO_2· fates under high-NO conditions, and instrumental setup. We attached following revised version:

The contribution of H-abstraction related products observed in this study was lower than that reported by Shen and coworkers, who reported a contribution of more than 70% (Shen et al., 2022). The experiments from the two studies were conducted in different chambers, under different conditions and with different instrumentations applied. Two chambers could introduce different wall losses of HOM, which can be further different between less oxygenated HOM and highly oxygenated HOM.

In this study the ·OH radicals were generated via photolysis of H_2O_2, whereas HONO photolysis was the main source of ·OH in Shen et al. (2022). The consecutive reaction between ·OH and H_2O_2 in our experiments leads to an enhanced production of HO_2· radicals, resulting in an HO_2· concentration of ~4 × 10^8 molecule cm^{-3}, which is approximately one order of magnitude higher than that reported by Shen et al. (2022). Also, the NO concentration in Shen et al. was constantly around ~20 ppb, while it was only ~7 ppb

before reaction in our study, resulting in a concentration of ~1 ppb during the early-reaction stage. Despite these differences, the contributions of RO_2· + NO reactions are dominant in both studies, accounting for more than 95% of RO_2· biomolecular losses under high-NO conditions. In addition, we did only consider early reaction stages, during which secondary oxidation was negligible and RO_2· chemistry was dominated by autoxidation and RO_2· + NO reactions. Therefore, the chemical system can be expected to be similar for both studies, at least under high-NO conditions. However, the constantly higher level of NO in the study by Shen et al. (2022) may continuously promote the H-abstraction channel.

The discrepancy may also arise from differences in measurement techniques: Shen et al. (2022) used an Eisele type inlet (Mauldin et al., 1999), while in this study a MION inlet was used (Rissanen et al., 2019). To compare both inlet systems, we conducted an experiment where both types of inlets were simultaneously used to measure the same oxidation systems. The reference system was α-pinene oxidation by ·OH, with the addition of NO (***Figure S17).*** The results indicate that the MION inlets detects a larger fraction of lesser oxygenated HOM (less than eight oxygen atoms) than the Eisele inlet, and that these HOM dominate the $C_{10}H_{17}O_x$·-related HOM family, while the relative contribution of higher oxygenated HOM (more than eight oxygen atoms) was larger in the study by Shen et al. (2022). When only the highly oxygenated HOM compounds are considered as was done in the study be Shen and coworkers, the relative contribution of $C_{10}H_{15}O_x$·-related HOM to the total HOM does increase to 64%. Therefore, a deeper comparison of the two inlet types may be of interest in the future but is outside the scope of this study.

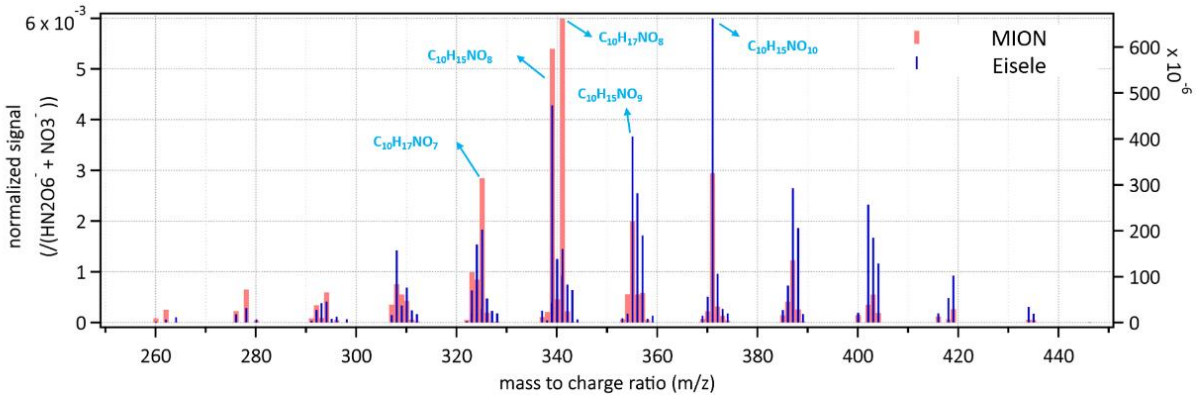

Figure S12. The signal of products derived from α-pinene oxidation with NO injection, detected by CIMS coupled with the MION (pink) and Eisele (blue) inlets.

Scientific Quality

The overall scientific quality is solid, as the hypothesis-experiment-interpretation logic does not show many shortcomings. There are two major comments I have.

> ***Comment 1:*** *Four-membered ring breakage with OH addition was mentioned in line 292, and the manuscript claimed the C10H17O7 unresponsiveness to NO change was due to this mechanism. There was no clear mechanism relationship explained in this manuscript and the paper referenced. A possible mechanistic interpretation is that the reaction rate of ring opening is fast with auto oxidation. This was partially mentioned in Lee et al., 2023., as the author stated the ring opening oxidation is a fast unimolecular reaction. This, however, is implicit, and the mechanistic linkage should be more explicitly developed within the manuscript.*

Responses:

We thank Shunyu Yao for this comment. We agreed with Shunyu Yao that this was not explained clearly enough in the previous version. The addition of an OH group to α-pinene can produce three isomers with the formula $C_{10}H_{17}O_3$. However, only one of these isomers will undergo subsequent autoxidation reactions after the four-member ring is opened (Xu et al., 2019). Furthermore, two subsequent autoxidation steps are needed to form $C_{10}H_{17}O_7$ peroxy radicals, and the rate constants of these autoxidation reactions are high enough to compete with biomolecule $RO_2\cdot$ reactions including $RO_2\cdot + NO$, $RO_2\cdot + HO_2\cdot$, and $RO_2\cdot + RO_2\cdot$. The rate constant of the $C_{10}H_{17}O_3$ autoxidation for forming $C_{10}H_{17}O_5$ is approximately 4 s^{-1}, while the $C_{10}H_{17}O_5$ autoxidation is even faster with approximately ~10 s^{-1} (Piletic and Kleindienst, 2022; Xu et al., 2019). For our experimental conditions the highest biomolecular reaction rate we could observe was ~1.88 s^{-1}, which is too low to efficiently compete with unimolecular reactions leading to the formation of $C_{10}H_{17}O_7$. Therefore, these previous studies can support our findings and we extended the discussion in the manuscript.

The updated discussion part is attached below:

The $C_{10}H_{17}O_7\cdot$ peroxy radicals exhibit a rapid formation rate and a high molar yield in α-pinene photooxidation systems, but their formation shows only a weak dependence on the NO concentration. Although ·OH addition to α-pinene yields three structural first-generation isomers ($C_{10}H_{17}O_3\cdot$), only the isomer that undergoes an opening of the four-membered ring forms a $C_{10}H_{17}O_3\cdot$ intermediate that is capable of subsequent autoxidation (Lee et al., 2023; Piletic and Kleindienst, 2022; Berndt et al., 2016). The ring-opened $C_{10}H_{17}O_3\cdot$ can then undergo two rapid unimolecular autoxidation steps, with a rate constant of approximately 4 s^{-1} for the first step which will lead to the formation of $C_{10}H_{17}O_5\cdot$, and a rate constant around 10 s^{-1} for the subsequent step and formation of $C_{10}H_{17}O_7\cdot$ species (Piletic and Kleindienst,

2022; Xu et al., 2019). The fast autoxidation steps of the resulting peroxy radicals imply that the characteristic timescales of their formation are significantly shorter than those of competing bimolecular reactions with NO, RO_2, and HO_2, whose maximum effective rates in our experiments range from 0.02 to 1.88 s^{-1} under NO-free, low-NO, and high-NO conditions, respectively. Therefore, biomolecular reactions, particularly involving NO, cannot effectively compete with the rapid autoxidation reactions, which can explain the observed weak NO dependence of the formation of $C_{10}H_{17}O_7^{\cdot}$-related HOM.

Comment 2: *The lack of explanation introduced another question. Both OH addition and H-abstraction followed by oxidation would form alkyl peroxy radical. However NO seems to only affect the formation of C10H15Ox, the product from H-abstraction. The author used unimolecular reaction rate as explanation, but it does not fully answer why the formation of alkyloxy radicals is selective through mechanistic interpretation. The referenced paper does show explicitly ring opening steps and reaction rate reported. I believe it would be more helpful to include such data in this manuscript. Referring to the 2022 science publication, there were three types of ring opening structures with the same molecular composition (C10H15O3). I think the author should give more explanation on that park as well.*

Responses:

We agree with Shunyu Yao that the key issue is not whether NO promotes alkoxy radical formation in general, but why the influence of NO appears to be stronger for products originating from the H-abstraction pathway than for those formed via OH addition. As will be discussed below, these differences likely arise from the distinct structural constraints of the corresponding alkoxy radicals. In the H-abstraction pathway, alkoxy radical formation is required to initiate the HOM autoxidation chain through successive ring-opening reactions, whereas HOM formation through the OH-addition pathway can proceed by opening the four-membered ring and subsequent autoxidation without involvement of NO. The results of this study show that contribution of fragments (C7) was more important for the H-abstraction pathway than for the OH-addition pathway, which suggests that either alkoxy radical formation or subsequent decomposition is more efficient in the H-abstraction pathway. According to Shen et al. (2022), three distinct $C_{10}H_{15}O_3$ isomers can be generated through different ring-opening sequences. Subsequent reactions of these intermediates with NO lead to different alkoxy radicals, which are expected to exhibit different affinities toward H-migration, O_2 addition, and decomposition. Since the present measurements only provide molecular formulas, the individual contributions of these isomers cannot be resolved. Nevertheless, their coexistence may contribute to the uncertainty of the fate of alkoxy radicals and thus explain the observed low sensitivity of the related HOM formation towards NO.

For a more detailed explanation and discussion we extended the manuscript in section 3.2 as follows:

As shown in ***Figure S12***, the summed abundance of C_7 families ($C_7H_{(10,12)}O_x$, $C_7H_{(9,11)}NO_x$), increase accordingly with the increase the NO injection, accounting for 0.01%, 0.3% and 2.4% of HOM compounds under NO-free, low-NO and high-NO conditions, respectively. It indicated increasing alkoxy radical decomposition with increasing NO. C_7 fragments are formed via dissociation of C_{10} alkoxy radicals derived from bimolecular reactions of C_{10} peroxy radicals with NO. Thus, the presence of NO promotes C_7 fragments by enhancing the production of alkoxy radicals (Vereecken and Peeters, 2000; Berndt, 2021). As the most abundant families, $C_7H_9NO_x$ and $C_7H_{11}NO_x$, likely originate from decomposition of $C_{10}H_{15}O_{x-1}\cdot$ and $C_{10}H_{17}O_{x-1}\cdot$, respectively. Under high-NO conditions, the ratio of $C_7H_9NO_x$ to $C_{10}H_{15}NO_x$ reached 0.22, substantially higher than the ratio of $C_7H_{11}NO_x$ to $C_{10}H_{17}NO_x$ (0.05). This observation suggests that either alkoxy radical formation or subsequent decomposition is more efficient in the H-abstraction pathway than in the ·OH-addition pathway.

Evidence for alkoxy radical H-migration is provided by the enhanced formation of $C_{10}H_{17}NO_7$ and $C_{20}H_{34}O_{11}$ under high-NO conditions (***Figure S9***). According to the oxygen-parity framework, $C_{10}H_{17}O_x\cdot$ radicals formed solely through autoxidation are expected to contain an odd number of oxygen atoms, whereas an alkoxy H-migration step changes the oxygen parity from odd to even (Kang et al., 2025). Thus, the observed increase in $C_{10}H_{17}NO_7$ and $C_{20}H_{34}O_{11}$ suggests the formation of $C_{10}H_{17}O_6\cdot$ peroxy radicals through at least one alkoxy radical isomerization step.

To initialize the HOM chain via OH-addition pathway, four-membered rings must open from chemically activated tertiary radicals, which is independent of NO (Xu et al., 2019). In contrast, HOM formation through the H-abstraction pathway requires NO. The initially formed peroxy radicals ($C_{10}H_{15}O_2\cdot$) are unlikely to undergo autoxidation directly; therefore, their reaction with NO to form alkoxy radicals ($C_{10}H_{15}O\cdot$), followed by the ring-opening step producing $C_{10}H_{15}O_3\cdot$ radicals, is necessary to initiate the HOM formation chain.

As autoxidation proceeds, higher oxygenated peroxy radicals, such as $C_{10}H_{17}O_x\cdot$ and $C_{10}H_{15}O_x\cdot$, are formed from $C_{10}H_{17}O_3\cdot$ and $C_{10}H_{15}O_4\cdot$, respectively. These peroxy radicals can further react with NO, yielding either the corresponding alkoxy radicals ($C_{10}H_{17}O_{x-1}$ and $C_{10}H_{15}O_{x-1}$) or organic nitrates ($C_{10}H_{17}NO_{x+1}$ and $C_{10}H_{15}NO_{x+1}$). However, the branching ratio between these two channels remains poorly constrained, contributing substantial uncertainty to the role of NO in HOM formation. Once formed, the fate of alkoxy radicals strongly depends on alkoxy radical structure (Vereecken and Peeters, 2010, 2009). Regardless of whether the precursor $RO_2\cdot$ radicals originate from the ·OH-addition or H-abstraction pathway, their subsequent chemistry can proceed through alkoxy radical intermediates. Therefore, the fate of these alkoxy radicals ultimately determines the impact of NO on HOM formation.

Overall, NO does influence HOM formation through alkoxy-radical chemistry. By promoting the conversion of $RO_2\cdot$ radicals to $RO\cdot$ radicals, NO initializes pathways for H-migration and decomposition

that would otherwise be less important. The extent to which these processes enhance or suppress HOM formation depends strongly on the structures of both the peroxy and alkoxy radicals, introducing substantial uncertainty into the overall role of NO.

1. ***Presentation Quality***

The presentation quality of this manuscript is decent, with good paragraph structures, informative figures and mostly clear logical reasoning. I think figures can be improved with following comments:

Fig 1 should adopt structure-based illustrations to visualize free radical position and ring opening step.

Explanation between result and interpretation was compressed and information lacking. There are many cases where the author offered little to none detailed logic to obtain conclusions. This was briefly mentioned in the scientific quality part, but lack of explanation also hinders readers' interpretation of results.

Many terms are overly abbreviated, which creates confusion. For example, reaction conditions can have a full name instead of labeled as AN or PN. Reactions can also be written out instead of assigned identifiers in the very beginning of the manuscript.

Responses:

We thank Shunyu Yao for these comments and the suggestions to improve the figures. We have made several modifications accordingly.

1. A figure illustrating the structure of molecules and free radical positions was added, as shown in ***Figure S1***. It can help to understand the explanations for the reaction mechanisms in the following sections.

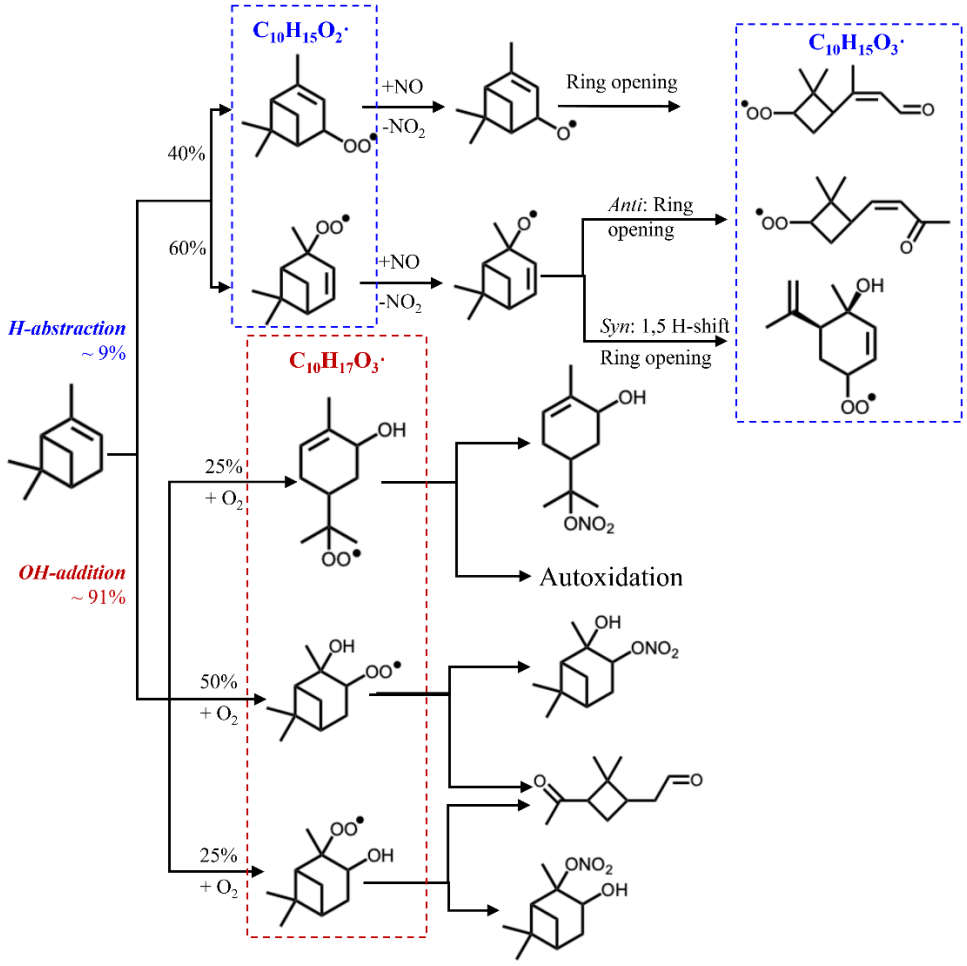

Figure S1. Formation pathways to form $C_{10}H_{15}O_3\cdot$ peroxy radicals through the H-abstraction channel and o form $C_{10}H_{17}O_3\cdot$ peroxy radicals through the OH-addition channel, derived from ·OH initiated α-pinene oxidation (Shen et al., 2022; Xu et al., 2019; Berndt et al., 2016).

2. Discussion was extended throughout the paper to link the observations and conclusions. Please find details in the ***responses*** to ***scientific significance and scientific quality part***.
3. All the abbreviations were replaced by full name throughout the paper:

   A0 was replaced by α-pinene (NO-free)

   AN_{low} was replaced by α-pinene (low-NO)

   AN_{high} was replaced by α-pinene (high-NO)

   P0 was replaced by pinonaldehyde (NO-free)

   PN_{high} was replaced by pinonaldehyde (high-NO)

   The changes can be found in ***Table 1***:

Table 1. Overview of experimental conditions: pinonaldehyde photooxidation without NO (NO-free) and with high NO (high-NO), α-pinene photooxidation without NO (NO-free), with low NO (low-NO), and with high NO (high-NO). The precursor concentrations in the dark and in photooxidation steady-state

conditions are shown at t_0 and t_S, respectively. The measurement uncertainty is less than 5%. Details about how to estimate ·OH and HO_2· radicals are given in Section 2.2.

		VOC		NO	·OH	HO_2·
		pinonaldehyde (ppbv)	α-pinene (ppbv)	(ppbv)	(# cm^{-3})	(# cm^{-3})
Pinonaldehyde (NO-free)	t_0	1.5	-	0	-	-
	t_S	0.75	-	0	6.5×10^6	6.4×10^8
Pinonaldehyde (high-NO)	t_0	1.8	-	7.0±0.13	-	-
	t_S	0.75	-	0.36±0.01	9.3×10^6	2.7×10^8
α-pinene (NO-free)	t_0	-	10.3±1.7	0	-	-
	t_S	0.01	8.3±1.4	0	1.25×10^6	3.1×10^8
α-pinene (low-NO)	t_0	-	11.1±1.3	0.91±0.05	-	-
	t_S	0.05	5.5±1.7	0.05±0.01	5.1×10^6	9.8×10^8
α-pinene (high-NO)	t_0	-	10.6±1.3	7.4±0.05	-	-
	t_S	0.09	4.2±2.1	0.16±0.01	7.5×10^6	1.0×10^9

Minor comments:

In Line 230, "with low NO (Anslow), and with high NO (Anlo)." Second Anlo should be ANhigh.

Responses:

Thanks for pointing out this mistake, it has been corrected.

In line 199, define ncps.

Responses:

Thanks for this comment, we now introduce this abbreviation properly:

A linear fit was applied to normalized HO_2·/[Br^- +(H_2O)Br^-] (in normalized counts per second, ncps) and modeled $[HO_2\cdot]_S$ (***Figure S4***), and the slope was used as calibration factor for calculating HO_2· levels in subsequent experiments (***Table 1***).

Line 369 "need longest time be formed." Consider rephrasing into longest formation time.

Responses:

Thanks for this comment, sentence was rephrased.

Hyphenation inconsistency, as an example both low-NO and low NO appeared.

Responses:

Thanks for this comment, all abbreviations and hyphenations have been corrected and should be now consistent throughout the manuscript.

References:

Baker, Y., Kang, S., Wang, H., Wu, R., Xu, J., Zanders, A., He, Q., Hohaus, T., Ziehm, T., Geretti, V., Bannan, T. J., O'Meara, S. P., Voliotis, A., Hallquist, M., McFiggans, G., Zorn, S. R., Wahner, A., and Mentel, T. F.: Impact of HO2⁄RO2 ratio on highly oxygenated α-pinene photooxidation products and secondary organic aerosol formation potential, Atmos. Chem. Phys., 24, 4789-4807, 10.5194/acp-24-4789-2024, 2024.

Berndt, T.: Peroxy Radical Processes and Product Formation in the OH Radical-Initiated Oxidation of alpha-Pinene for Near-Atmospheric Conditions, J Phys Chem A, 125, 9151-9160, 10.1021/acs.jpca.1c05576, 2021.

Berndt, T., Richters, S., Jokinen, T., Hyttinen, N., Kurten, T., Otkjaer, R. V., Kjaergaard, H. G., Stratmann, F., Herrmann, H., Sipila, M., Kulmala, M., and Ehn, M.: Hydroxyl radical-induced formation of highly oxidized organic compounds, NATURE COMMUNICATIONS, 7, 10.1038/ncomms13677, 2016.

Kang, S., Wildt, J., Pullinen, I., Vereecken, L., Wu, C., Wahner, A., Zorn, S. R., and Mentel, T. F.: Formation of highly oxygenated organic molecules from α-pinene photooxidation: evidence for the importance of highly oxygenated alkoxy radicals, EGUsphere, 2025, 1-33, 10.5194/egusphere-2025-2772, 2025.

Lee, B. H., Iyer, S., Kurtén, T., Varelas, J. G., Luo, J., Thomson, R. J., and Thornton, J. A.: Ring-opening yields and auto-oxidation rates of the resulting peroxy radicals from OH-oxidation of α-pinene and β-pinene, Environmental Science: Atmospheres, 3, 399-407, 10.1039/d2ea00133k, 2023.

Mauldin, R. L., Tanner, D. J., Heath, J. A., Huebert, B. J., and Eisele, F. L.: Observations of H2SO4and MSA during PEM-Tropics-A, Journal of Geophysical Research: Atmospheres, 104, 5801-5816, 10.1029/98jd02612, 1999.

Piletic, I. R. and Kleindienst, T. E.: Rates and Yields of Unimolecular Reactions Producing Highly Oxidized Peroxy Radicals in the OH-Induced Autoxidation of alpha-Pinene, beta-Pinene, and Limonene, J Phys Chem A, 126, 88-100, 10.1021/acs.jpca.1c07961, 2022.

Shen, H., Vereecken, L., Kang, S., Pullinen, I., Fuchs, H., Zhao, D., and Mentel, T. F.: Unexpected significance of a minor reaction pathway in daytime formation of biogenic highly oxygenated organic compounds, Science Advances, 8, eabp8702, doi:10.1126/sciadv.abp8702, 2022.

Vereecken, L. and Peeters, J.: Theoretical Study of the Formation of Acetone in the OH-Initiated Atmospheric Oxidation of α-Pinene, The Journal of Physical Chemistry A, 104, 11140-11146, 10.1021/jp0025173, 2000.

Vereecken, L. and Peeters, J.: Decomposition of substituted alkoxy radicals--part I: a generalized structure-activity relationship for reaction barrier heights, Phys Chem Chem Phys, 11, 9062-9074, 10.1039/b909712k, 2009.

Vereecken, L. and Peeters, J.: A structure-activity relationship for the rate coefficient of H-migration in substituted alkoxy radicals, Phys Chem Chem Phys, 12, 12608-12620, 10.1039/c0cp00387e, 2010.

Xu, L., Moller, K. H., Crounse, J. D., Otkjaer, R. V., Kjaergaard, H. G., and Wennberg, P. O.: Unimolecular Reactions of Peroxy Radicals Formed in the Oxidation of alpha-Pinene and beta-Pinene by Hydroxyl Radicals, J Phys Chem A, 123, 1661-1674, 10.1021/acs.jpca.8b11726, 2019.